ASC Report No. 01/2007

Simple A Posteriori Error Estimators for the h-Version of the Boundary Element Method

Samuel Ferraz-Leite, Dirk Praetorius

Institute for Analysis and Scientific Computing
Vienna University of Technology — TU Wien
www.asc.tuwien.ac.at ISBN 978-3-902627-00-1

Institute for Analysis and Scientific Computing
Vienna University of Technology
Wiedner Hauptstraße 8–10
1040 Wien, Austria

E-Mail: admin@asc.tuwien.ac.at
WWW: http://www.asc.tuwien.ac.at
FAX: +43-1-58801-10196

ISBN 978-3-902627-00-1

ASC
TU WIEN

SIMPLE A POSTERIORI ERROR ESTIMATORS FOR THE h-VERSION OF THE BOUNDARY ELEMENT METHOD

SAMUEL FERRAZ-LEITE AND DIRK PRAETORIUS

ABSTRACT. The h-$h/2$-strategy is one well-known technique for the a posteriori error estimation for Galerkin discretizations of energy minimization problems. One considers $\eta_H := \|\phi_{h/2} - \phi_h\|$ to estimate the error $\|\phi - \phi_h\|$, where ϕ_h is a Galerkin solution with respect to a mesh $\mathcal{T}_h$ and $\phi_{h/2}$ is a Galerkin solution with respect to the mesh $\mathcal{T}_{h/2}$ obtained from a uniform refinement of $\mathcal{T}_h$. This error estimator is always efficient and observed to be also reliable in practice. However, for boundary element methods, the energy norm is non-local and thus the error estimator η_H does not provide information for a local mesh-refinement. We consider Symm's integral equation of the first kind, where the energy space is the negative-order Sobolev space $\widetilde{H}^{-1/2}(\Gamma)$. Recent localization techniques allow to replace the energy norm in this case by some weighted L^2-norm. Then, this very basic error estimation strategy is also applicable to steer an h-adaptive algorithm. Numerical experiments in 2D and 3D show that the proposed method works well in practice. A short conclusion is concerned with other integral equations, e.g., the hypersingular case with energy space $\widetilde{H}^{1/2}(\Gamma)$ and $H_0^{1/2}(\Gamma)$, respectively, or a transmission problem.

Dedicated to Professor Ernst P. Stephan on the occasion of his 60th birthday

1. Introduction and Model Example

We consider Symm's integral equation

$$V\phi = f \quad \text{on } \Gamma \tag{1.1}$$

for a relatively open subset $\Gamma \subseteq \partial\Omega$ of the boundary of a bounded Lipschitz domain $\Omega \subseteq \mathbb{R}^d$, for $d = 2, 3$. Here, $V\phi$ denotes the simple-layer potential

$$V\phi(x) = \int_\Gamma G(x-y)\phi(y)\,ds_y \quad \text{for } x \in \Gamma \tag{1.2}$$

with $G(\cdot)$ the fundamental solution of the Laplacian, i.e.

$$G(z) = \begin{cases} -\frac{1}{2\pi}\log|z| & \text{for } d = 2, \\ +\frac{1}{4\pi}|z|^{-1} & \text{for } d = 3, \end{cases} \tag{1.3}$$

and with $\int_\Gamma ds$ the integration over the surface piece Γ. The operator $V : \widetilde{H}^{-1/2}(\Gamma) \to H^{1/2}(\Gamma)$ is an elliptic isomorphism between the fractional-order Sobolev space $\mathcal{H} := \widetilde{H}^{-1/2}(\Gamma)$ and its dual $\mathcal{H}^* = H^{1/2}(\Gamma)$, where we additionally assume $\operatorname{diam}(\Omega) < 1$ in case of $d = 2$. It

Date: 27.07.2007, **22.07.2008 (revised version)**.

1991 *Mathematics Subject Classification.* 65N38,65R20,65N50.

Key words and phrases. Symm's integral equation, hypersingular integral equation, boundary element method, Galerkin method, a posteriori error estimate, adaptive algorithm.

thus provides an equivalent scalar product $\langle\!\langle \cdot\,, \cdot \rangle\!\rangle$ on the energy space $\mathcal{H}$ defined by $\langle\!\langle \phi\,, \psi \rangle\!\rangle := \langle V\phi\,, \psi\rangle$. Here, the duality brackets $\langle \cdot\,, \cdot\rangle$ extend the $L^2(\Gamma)$-scalar product. We denote by $|\!|\!| \cdot |\!|\!|$ the induced energy norm.

The right-hand side $f \in \mathcal{H}^*$ in (1.1) may either stem from an indirect approach or from direct integral formulations. In the latter case, f takes the form $f = (K + 1/2)g$ with K the double-layer potential operator and $g \in \mathcal{H}^*$ some known Dirichlet data.

Given $f \in \mathcal{H}^*$, the unique solution $\phi \in \mathcal{H}$ of (1.1) solves

$$\langle\!\langle \phi\,, \psi \rangle\!\rangle = \langle f\,, \psi\rangle \quad \text{for all } \psi \in \mathcal{H}. \tag{1.4}$$

Let $\mathcal{T}_h$ be a triangulation of Γ (with local mesh-size h). Then, the lowest-order Galerkin method is to find a $\mathcal{T}_h$-piecewise constant function $\phi_h \in \mathcal{P}^0(\mathcal{T}_h)$ which solves the weak form

$$\langle\!\langle \phi_h\,, \psi_h \rangle\!\rangle = \langle f\,, \psi_h\rangle \quad \text{for all } \psi_h \in \mathcal{P}^0(\mathcal{T}_h). \tag{1.5}$$

We stress the Galerkin orthogonality

$$\langle\!\langle \phi - \phi_h\,, \psi_h \rangle\!\rangle = 0 \quad \text{for all } \psi_h \in \mathcal{P}^0(\mathcal{T}_h), \tag{1.6}$$

which in fact characterizes the discrete solution ϕ_h. The goal of this work is to contribute to simple and accurate a posteriori estimation for the error $|\!|\!| \phi - \phi_h |\!|\!|$ in the energy norm: An a posteriori error estimator is a computable quantity η which does not depend on the (in general unknown) exact solution ϕ but only on computable data, e.g. the discrete solution ϕ_h, and which estimates the error $|\!|\!| \phi - \phi_h |\!|\!|$ in the energy norm. We aim to provide estimates

$$C_{\text{eff}}^{-1}\, \eta \le |\!|\!| \phi - \phi_h |\!|\!| \le C_{\text{rel}}\, \eta \tag{1.7}$$

which are referred to as efficiency (lower estimate) and reliability (upper estimate) of η, respectively. The constants $C_{\text{eff}}, C_{\text{rel}}$ may not depend on ϕ or ϕ_h, but on the given right-hand side $f \in \mathcal{H}^*$ as well as weakly on $\mathcal{T}_h$, e.g., on the shape of the elements in $\mathcal{T}_h$.

To introduce the analytical idea of this paper, let $\mathcal{T}_{h/2}$ be a second triangulation of Γ obtained from a uniform refinement of $\mathcal{T}_h$. We consider the discrete spaces $X_h := \mathcal{P}^0(\mathcal{T}_h)$ and $X_{h/2} := \mathcal{P}^0(\mathcal{T}_{h/2})$ with corresponding Galerkin solutions $\phi_h \in X_h$ and $\phi_{h/2} \in X_{h/2}$, respectively. Recall that the best approximation property of the Galerkin solution with respect to the energy norm and $X_h \subset X_{h/2}$ provide

$$|\!|\!| \phi - \phi_{h/2} |\!|\!| \le |\!|\!| \phi - \phi_h |\!|\!|. \tag{1.8}$$

In a first step, we now consider the h-$h/2$-error estimator

$$\eta_H := |\!|\!| \phi_{h/2} - \phi_h |\!|\!|. \tag{1.9}$$

The Galerkin orthogonality (1.6) for $X_{h/2}$ and $X_h \subset X_{h/2}$ yield

$$|\!|\!| \phi - \phi_h |\!|\!|^2 = |\!|\!| \phi - \phi_{h/2} |\!|\!|^2 + |\!|\!| \phi_{h/2} - \phi_h |\!|\!|^2 = |\!|\!| \phi - \phi_{h/2} |\!|\!|^2 + \eta_H^2$$

and thus $\eta_H \le |\!|\!| \phi - \phi_h |\!|\!|$. This proves efficiency of η_H with known efficiency constant $C_{\text{eff}} = 1$. The reliability of η_H is usually proven with the help of the *saturation assumption*, which is a strengthened version of (1.8) and reads

$$|\!|\!| \phi - \phi_{h/2} |\!|\!| \le C_{\text{sat}}\, |\!|\!| \phi - \phi_h |\!|\!| \tag{A}$$

with a constant $C_{\rm sat} \in (0,1)$ which is uniform with respect to the discretization parameter $h \to 0$. Under this assumption, we obtain $|||\phi - \phi_h|||^2 = |||\phi - \phi_{h/2}|||^2 + \eta_H^2 \le C_{\rm sat}^2\, |||\phi - \phi_h|||^2 + \eta_H^2$ and thus reliability

$$|||\phi - \phi_h||| \le \frac{1}{\sqrt{1 - C_{\rm sat}^2}}\, \eta_H. \tag{1.10}$$

The same arguments show that reliability of η_H, in fact, implies the saturation assumption (A). We state these observations in the following proposition for later reference. We stress that our considerations are, so far, independent of the precise mathematical setting, e.g., Symm's integral equation.

Proposition 1.1. (i) *The h-h/2-error estimator η_H is always efficient with $C_{\rm eff} = 1$.*
(ii) *Under the saturation assumption* (A)*, η_H is reliable with $C_{\rm rel} = 1/\sqrt{1 - C_{\rm sat}^2}$.*
(iii) *If η_H is reliable with constant $C_{\rm rel} > 0$, there holds* (A) *with $C_{\rm sat} = (1 - C_{\rm rel}^{-2})^{1/2}$.* □

For the finite element method, the saturation assumption (A) can be proven under some mild conditions on the local mesh refinement, cf. [10]. However, we stress that the saturation assumption — although observed in practice — has not been proven for the boundary element method, yet.

An additional difficulty for boundary element methods is the non-locality of the energy norm, e.g. $|||\cdot||| \sim \|\cdot\|_{\widetilde{H}^{-1/2}(\Gamma)}$ for Symm's integral equation. Here, non-locality of the norm means that $|||\cdot|||$ cannot be written as sum of local contributions — in contrast to, e.g., the L^2-norm which satisfies $\|\cdot\|_{L^2(\Gamma)}^2 = \sum_{T \in \mathcal{T}_h} \|\cdot\|_{L^2(T)}^2$. One therefore needs so-called localization techniques which provide lower and upper estimates for $|||\phi_{h/2} - \phi_h|||$ by use of, e.g., weighted L^2-norms. We use recent ideas from [5] to prove that, for shape-regular meshes,

$$\mu_H = \|h^{1/2}(\phi_{h/2} - \phi_h)\|_{L^2(\Gamma)} \tag{1.11}$$

is an equivalent error estimator, i.e. there are constants $C_1, C_2 > 0$ such that

$$C_1^{-1} \mu_H \le \eta_H \le C_2 \mu_H. \tag{1.12}$$

Here $h \in L^\infty(\Gamma)$, $h|_T := \operatorname{diam}(T)$ for $T \in \mathcal{T}_h$, denotes the local mesh-size function. For our numerical experiments, we thus may use the local contributions $\mu_{H,j} := \operatorname{diam}(T_j)^{1/2} \|\phi_{h/2} - \phi_h\|_{L^2(T_j)}$ to decide whether an element $T_j \in \mathcal{T}_h$ should be refined or not. We stress, that even though the localization techniques have been developed and used in [5], they have not been used to derive the localized h-$h/2$-error estimator which is a new contribution of this work. Moreover, the h-$h/2$-strategy — although simple and quite natural — has neither been proposed for error estimation nor for adaptive mesh-refinement in the context of boundary element methods, yet.

We conclude the introduction with some general remarks on the proposed method, which are discussed in more detail in Section 4–6 below: First, h-$h/2$ error estimation can be used within a general framework and is, in particular, applicable to direct or indirect boundary integral formulations. Second, there is almost no implementational overhead: The computation of η_H only uses the Galerkin matrix, whereas μ_H only needs the computation of a weighted L^2-norm of piecewise constant functions. Third, only the Galerkin matrix $\mathbf{A}_{h/2}$ with respect to $\mathcal{T}_{h/2}$ has to be built. Then, both Galerkin solutions $\phi_{h/2}$ and ϕ_h can be computed simultaneously, cf. Section 4.1. By use of certain matrix compression techniques

and fast solvers the *additional cost* for the computation of the estimator η_H, i.e. the computation of $\phi_{h/2}$, is almost bounded by a factor 3 in three dimensions. In the two dimensional case, the *additional cost* for the computation of η_H is only of the same complexity as the computation of the Galerkin solution ϕ_h. Fourth, the numerical experiments give empirical evidence that η_H is reliable and efficient and that the error estimation $\eta_H \approx |\!|\!| \phi - \phi_h |\!|\!|$ is very accurate. Finally, recent techniques allow to prove convergence of the μ_H-steered adaptive BEM [14]. On the other hand, we admit that the analysis strongly depends on the saturation assumption (A). From the mathematical point of view, this can be seen as a major disadvantage.

The remaining contents of this paper are organized as follows: In Section 2 we recall some notations and restrictions for the triangulations under consideration. In Section 3, we provide the localization of the energy norm in case of Symm's integral equation. Details on the implementation of η_H and μ_H are found in Section 4. We stress that our analysis, so far, is restricted to the case of isotropic mesh-refinement in 3D, whereas anisotropic mesh-refinement is necessary to resolve edge-singularities efficiently. We thus give some heuristics for a μ_H-steered adaptive algorithm which leads to anisotropic meshes. Numerical experiments in 2D and 3D are found in Section 5. These underline that the developed techniques and proposed algorithms are even capable to control the Galerkin error in case of both, isotropic and anisotropic mesh-refinement. Some concluding remarks are drawn in Section 6 and we outline at least some further applications of the proposed method.

2. Preliminaries

General Triangulations and Piecewise Polynomials. Let $\mathcal{T}_h = \{T_1, \dots, T_N\}$ be a triangulation of Γ, i.e.

- $\overline{\Gamma} = \bigcup_{j=1}^N T_j$, i.e. $\mathcal{T}_h$ covers $\overline{\Gamma}$,
- each $T_j \in \mathcal{T}_h$ is closed and non-degenerate, i.e. $|T_j| > 0$,
- $|T_j \cap T_k| = 0$ for the intersection of two elements $T_j, T_k \in \mathcal{T}_h$ with $T_j \neq T_k$.

Here, $|\cdot|$ denotes the $(d-1)$-dimensional surface measure. For the ease of presentation, we assume that, for $d = 2$, the elements $T_j \in \mathcal{T}_h$ are affine boundary pieces. For $d = 3$, the elements $T_j \in \mathcal{T}_h$ are assumed to be either flat triangles or flat rectangles, respectively. For $p \geq 0$, we denote by $\mathcal{P}^p(\mathcal{T}_h)$ the space of all $\mathcal{T}_h$-piecewise polynomials. As usual, these discrete functions are defined on a reference element T^{ref} and mapped onto the respective elements by affine transformations. The reference element is given by $T^{\text{ref}}_{2D} = [0,1]$ in case of $d = 2$, and either $T^{\text{ref}}_{3D,\triangle} = \text{conv}\{(0,0),(0,1),(1,0)\}$ or $T^{\text{ref}}_{3D,\square} = [0,1]^2$ in case of $d = 3$. Only in the latter case, $\mathcal{P}^p(\mathcal{T}_h)$ contains polynomials of partial degree $\leq p$. In the other cases p denotes the maximal total degree.

Local Mesh-Widths and K-Mesh Property. For each element $T_j \in \mathcal{T}_h$, we define the diameter $h_j := \text{diam}(T_j) > 0$. Moreover, let $\varrho_j > 0$ be the diameter of the largest sphere centered at a point in T_j, whose intersection with Γ lies entirely inside T_j. To deal with error estimates on adaptively refined meshes, we define local mesh-width functions $h, \varrho \in L^\infty(\Gamma)$ by $h|_{T_j} := h_j$ and $\varrho|_{T_j} := \varrho_j$ for $T_j \in \mathcal{T}_h$, respectively. Obviously, there holds $\varrho = h$ pointwise for $d = 2$, whereas only $\varrho \leq h$ for $d = 3$. We thus define the shape-regularity constant

$$\sigma(\mathcal{T}_h) := \sup_{T_j \in \mathcal{T}_h} (h_j/\varrho_j) = \|h/\varrho\|_{L^\infty(\Gamma)} \geq 1. \tag{2.1}$$

By definition, there holds the pointwise estimate $\varrho \le h \le \sigma(\mathcal{T}_h)\varrho$, with $\sigma(\mathcal{T}_h) = 1$ for $d = 2$.

A mesh-refinement strategy, which yields a sequence $(\mathcal{T}_h^{(\ell)})$ of triangulations, is called *isotropic*, provided that $\sigma_0 := \sup_{\ell\in\mathbb{N}} \sigma(\mathcal{T}_h^{(\ell)}) < \infty$. However, in 3D the mesh-refinement strategies of practical interest often lead to an anisotropic mesh-refinement. More precisely, the adaptive meshes obtained below satisfy the K-mesh property for some constant $\kappa(\mathcal{T}_h) \ge 1$, i.e. there hold:

- For any $T_j, T_k \in \mathcal{T}_h$ with $T_j \cap T_k \neq \emptyset$ holds $h_j/h_k \le \kappa(\mathcal{T}_h)$ as well as $\varrho_j/\varrho_k \le \kappa(\mathcal{T}_h)$, i.e. the local mesh-widths of neighbouring elements do not vary too rapidly.
- For any node $z \in \overline{\Gamma}$ of $\mathcal{T}_h$ holds $\#\{T \in \mathcal{T}_h : z \in T\} \le \kappa(\mathcal{T}_h)$, i.e. each node does not belong to too many elements of $\mathcal{T}_h$.

We stress that the estimates below depend on (an upper bound of) the mesh-constant $\kappa(\mathcal{T}_h)$.

Regular Meshes vs. Hanging Nodes. We recall that the triangulation $\mathcal{T}_h$ is *regular* in the sense of Ciarlet, if, for all elements $T_j, T_k \in \mathcal{T}_h$ with $T_j \neq T_k$, the intersection $T_j \cap T_k$

- is either empty,
- or a vertex of both T_j and T_k,
- or an edge of both T_j and T_k.

These properties are needed to ensure global continuity and thus H^1-conformity of certain $\mathcal{T}_h$-piecewise polynomials.

However, for the analysis of Symm's integral equation we may deal with discontinuous $\mathcal{T}_h$-piecewise polynomials to discretize the energy space $\widetilde{H}^{-1/2}(\Gamma)$. In this case, we thus drop the regularity assumption and allow hanging nodes instead. For the analysis, we shall assume that $\mathcal{T}_h$ is *almost regular*, i.e. there is a regular triangulation $\widehat{\mathcal{T}}_h$ of Γ such that

- $\widehat{\mathcal{T}}_h$ is obtained from certain refinements of $\mathcal{T}_h$, i.e. $\mathcal{P}^0(\mathcal{T}_h) \subseteq \mathcal{P}^0(\widehat{\mathcal{T}}_h)$,
- there is a constant $\widehat{\kappa}(\mathcal{T}_h)$, which only depends on $\mathcal{T}_h$ such that

$$\kappa(\widehat{\mathcal{T}}_h) \le \widehat{\kappa}(\mathcal{T}_h)\,\kappa(\mathcal{T}_h) \tag{2.2}$$

and that

$$\widehat{h} \le h \le \widehat{\kappa}(\mathcal{T}_h)\,\widehat{h} \quad \text{as well as} \quad \widehat{\varrho} \le \varrho \le \widehat{\kappa}(\mathcal{T}_h)\,\widehat{\varrho}. \tag{2.3}$$

Here, h and ϱ as well as $\widehat{h}$ and $\widehat{\varrho}$ denote the mesh-width functions with respect to $\mathcal{T}_h$ and $\widehat{\mathcal{T}}_h$, respectively.

We stress that both assumptions hold for the 3D experiments provided below.

3. Symm's Integral Equation

For the entire section, let $\mathcal{T}_h$ be an almost-regular triangulation of Γ. We adopt the notations of the introductory section. The first lemma provides a localization of the $\widetilde{H}^{-1/2}$-norm for discrete functions $v_h \in L^2(\Gamma)$. This localization is naturally given in terms of a mesh-size weighted L^2-norm. The inverse estimate (3.1) is proven in [15]. The approximation estimates (3.2)–(3.3) are taken from [5].

Lemma 3.1. (i) *For any discrete function $v_h \in \mathcal{P}^0(\mathcal{T}_h)$ holds the inverse estimate*

$$\|\varrho^{1/2} v_h\|_{L^2(\Gamma)} \le C_3 |\!|\!| v_h |\!|\!|, \tag{3.1}$$

where the constant $C_3 > 0$ only depends on Γ and the mesh-constants $\kappa(\mathcal{T}_h)$ and $\widehat{\kappa}(\mathcal{T}_h)$.
(ii) *For Π_h the L^2-projection onto $\mathcal{P}^0(\mathcal{T}_h)$ and any $v \in L^2(\Gamma)$ holds*

$$|||v - \Pi_h v||| \le C_4 \|h^{1/2}(v - \Pi_h v)\|_{L^2(\Gamma)} \le C_4 \|h^{1/2} v\|_{L^2(\Gamma)}. \tag{3.2}$$

The constant $C_4 > 0$ only depends on Γ but not on the triangulation $\mathcal{T}_h$.
(iii) *For $\mathbb{G}_h$ the Galerkin projection onto $\mathcal{P}^0(\mathcal{T}_h)$ and any $v \in L^2(\Gamma)$ holds*

$$|||v - \mathbb{G}_h v||| \le C_4 \min\big\{\|h^{1/2}(v - \mathbb{G}_h v)\|_{L^2(\Gamma)}, \|h^{1/2} v\|_{L^2(\Gamma)}\big\}. \tag{3.3}$$

(iv) *Neither of the constants C_3 and C_4 depend on the local mesh-sizes h and ϱ or on the number $\#\mathcal{T}_h$ of elements.* □

Sketch of Proof. Let $\widehat{\mathcal{T}}_h$ be the regular triangulation corresponding to $\mathcal{T}_h$ in the sense of the preliminary section. According to [15, Theorem 3.6], there holds

$$\|\varrho^{1/2} v_h\|_{L^2(\Gamma)} \le C_3 |||v_h||| \quad \text{for all } v_h \in \mathcal{P}^0(\widehat{\mathcal{T}}_h),$$

where the constant $C_3 > 0$ depends only on $\kappa(\widehat{\mathcal{T}}_h)$ and thus on $\kappa(\mathcal{T}_h)$ and $\widehat{\kappa}(\mathcal{T}_h)$. In particular, (i) follows from $\mathcal{P}^0(\mathcal{T}_h) \subseteq \mathcal{P}^0(\widehat{\mathcal{T}}_h)$. (In [15] the local mesh-width is a certain nodal $\mathcal{P}^1$ interpolant of the local mesh-width ϱ defined here. Both definitions are equivalent up to the multiplicative constant $\kappa(\widehat{\mathcal{T}}_h)$.) (ii) is proven in [5, Theorem 4.1]. Therefore, the best approximation property of the Galerkin projection yields, for $v \in L^2(\Gamma)$,

$$|||v - \mathbb{G}_h v||| \le |||v - \Pi_h v||| \le C_4 \|h^{1/2} v\|_{L^2(\Gamma)}.$$

Defining, $w := v - \mathbb{G}_h v \in L^2(\Gamma)$ and observing $w - \mathbb{G}_h w = v - \mathbb{G}_h v$, we additionally obtain

$$|||v - \mathbb{G}_h v||| = |||w - \mathbb{G}_h w||| \le C_4 \|h^{1/2} w\|_{L^2(\Gamma)} = C_4 \|h^{1/2}(v - \mathbb{G}_h v)\|_{L^2(\Gamma)}.$$

The combination of the latter estimates proves (iii). □

***Remark* 1.** For the ease of presentation, we restrict to the lowest-order case. We stress that (3.2)–(3.3) hold under some richness assumptions on the discrete space X_h. Namely, we have to assume that $\Pi_h : L^2(\Gamma) \to X_h$ is the L^2-projection and that X_h contains at least either $\mathcal{P}^0(\mathcal{T}_h)$ or $\mathcal{P}^1(\mathcal{T}_h) \cap C(\Gamma)$, where in the latter case C_4 additionally depends on the shape-regularity constant $\sigma(\mathcal{T}_h)$, cf. [5]. The lower localization estimate (3.1) holds for any $\widehat{\mathcal{T}}_h$-piecewise polynomial $v_h \in \mathcal{P}^p(\widehat{\mathcal{T}}_h)$, where the constant C_3 depends on the polynomial degree p and on the mesh-constant $\kappa(\widehat{\mathcal{T}}_h)$, cf. [15]. The dependence of C_3 and C_4 on Γ follows from equivalence of norms $|||\cdot||| \sim \|\cdot\|_{\widetilde{H}^{-1/2}(\Gamma)}$. □

Theorem 3.2. *The a posteriori error estimator*

$$\mu_H := \|\varrho^{1/2}(\phi_{h/2} - \phi_h)\|_{L^2(\Gamma)} \tag{3.4}$$

satisfies

$$(\sqrt{2}\, C_3)^{-1} \mu_H \le \eta_H \le C_4\, \sigma(\mathcal{T}_h)^{1/2}\, \mu_H \tag{3.5}$$

with the constants $C_3, C_4 > 0$ from Lemma 3.1. In particular, μ_H is always efficient.

Proof. Let $\mathbb{G}_h$ denote the Galerkin projection onto $\mathcal{P}^0(\mathcal{T}_h)$ and note that $\mathcal{P}^0(\mathcal{T}_h) \subset \mathcal{P}^0(\mathcal{T}_{h/2})$ implies $\mathbb{G}_h \phi_{h/2} = \phi_h$. Therefore, we have $\phi_{h/2} - \phi_h = (1 - \mathbb{G}_h)(\phi_{h/2} - \phi_h)$. Now, (3.3) proves

$$|||\phi_{h/2} - \phi_h||| = |||(1 - \mathbb{G}_h)(\phi_{h/2} - \phi_h)||| \le C_4 \|h^{1/2}(\phi_{h/2} - \phi_h)\|_{L^2(\Gamma)} \le C_4 \|(h/\varrho)^{1/2}\|_{L^\infty(\Gamma)}\, \mu_H.$$

By definition, there holds $\sigma(\mathcal{T}_h)^{1/2} = \|(h/\varrho)^{1/2}\|_{L^\infty(\Gamma)}$, which leads to the upper estimate in (3.5). For the lower estimate, we use the inverse estimate (3.1) on $\mathcal{P}^0(\mathcal{T}_{h/2})$ to obtain

$$\|(\varrho/2)^{1/2}(\phi_{h/2} - \phi_h)\|_{L^2(\Gamma)} \le C_3 \, |||\phi_{h/2} - \phi_h|||,$$

which concludes the proof. □

***Remark* 2.** Theorem 3.2 states equivalence of η_H and μ_H in case of either $d = 2$ or isotropic mesh-refinement in case of $d = 3$. However, the numerical experiments below indicate that the critical estimate $\eta_H \lesssim \mu_H$ does even hold for anisotropic mesh-refinement. □

The following algorithm realizes an adaptive mesh-refining strategy based on the localized h-$h/2$-error estimator μ_H.

Algorithm 3.3. *Let $\varepsilon > 0$ be a given tolerance and $\theta \in (0, 1)$ the adaptivity parameter. Given $\ell := 0$ and an initial mesh $\mathcal{T}_h^{(0)}$, do the following:*

(i) *Refine $\mathcal{T}_h^{(\ell)}$ uniformly to obtain $\mathcal{T}_{h/2}^{(\ell)}$.*

(ii) *Compute Galerkin solutions $\phi_h^{(\ell)} \in \mathcal{P}^0(\mathcal{T}_h^{(\ell)})$ and $\phi_{h/2}^{(\ell)} \in \mathcal{P}^0(\mathcal{T}_{h/2}^{(\ell)})$.*

(iii) *Compute error estimator $\eta_H := |||\phi_{h/2}^{(\ell)} - \phi_h^{(\ell)}|||$ and stop provided $\eta_H \le \varepsilon$.*

(iv) *Compute refinement indicators $\mu_{H,j} := \varrho_j^{1/2} \|\phi_{h/2}^{(\ell)} - \phi_h^{(\ell)}\|_{L^2(T_j)}$ for $\mathcal{T}_h^{(\ell)} = \{T_1, \dots, T_N\}$.*

(v) *Determine set $\mathcal{M}_h^{(\ell)} \subseteq \mathcal{T}_h^{(\ell)}$ of minimal cardinality such that*

$$\theta \sum_{T_j \in \mathcal{T}_h^{(\ell)}} \mu_{H,j}^2 \le \sum_{T_j \in \mathcal{M}_h^{(\ell)}} \mu_{H,j}^2. \tag{3.6}$$

(vi) *Refine the marked elements $\mathcal{M}_h^{(\ell)}$ to obtain a new mesh $\mathcal{T}_h^{(\ell+1)}$.*

(vii) *Update $\ell \mapsto \ell + 1$, and go to* (i). □

***Remark* 3.** We stress that we do some additional marking in (v) to guarantee that

$$\kappa(\mathcal{T}_h^{(\ell)}) \le C_5 \quad \text{as well as} \quad \widehat{\kappa}(\mathcal{T}_h^{(\ell)}) \le C_5$$

with a constant $C_5 > 0$ that only depends on $\mathcal{T}_h^{(0)}$ but not on ℓ. We refer to Section 4.3–4.5 below for details. — For instance, in 2D, let T_j and T_k be two neighbouring elements. If T_k is marked for refinement and $h_j > h_k$, we also mark T_j for refinement. By this procedure, we guarantee that $\kappa(\mathcal{T}_h^{(\ell)}) \le 2\,\kappa(\mathcal{T}_h^{(0)})$ is uniformly bounded as $\ell \to \infty$. □

***Remark* 4.** The marking criterion (3.6) was introduced in [9] to prove convergence of an adaptive algorithm for some P1-FEM for the Laplace equation. In the context of the boundary element method, the mathematical proof of convergence and optimality of adaptive algorithms is widely open. Only recently, it could be proven that —under the saturation assumption (A) — Algorithm 3.3 yields convergence of the discrete solutions $\phi_h^{(\ell)}$ towards the exact solution $\phi \in \widetilde{H}^{-1/2}(\Gamma)$ for any choice of $\theta \in (0, 1)$, cf. [14]. For the numerical experiments below, we always used $\theta = 0.5$ for adaptive mesh-refinement. □

When Algorithm 3.3 stops with $\eta_H \le \varepsilon$, the Galerkin solution $\phi_{h/2}^{(\ell)}$ is a better approximation of ϕ than $\phi_h^{(\ell)}$ as $|||\phi - \phi_{h/2}^{(\ell)}||| \le |||\phi - \phi_h^{(\ell)}|||$. Thus, Algorithm 3.3 should usually return

$\phi_{h/2}^{(\ell)}$ instead of $\phi_h^{(\ell)}$. From this point of view, the quantity ϕ_h becomes a temporary result only. One usually aims to compute side results with as less computational effort as possible. In our case, we can simply avoid to compute ϕ_h as follows:

Theorem 3.4. *With $\Pi_h : L^2(\Gamma) \to \mathcal{P}^0(\mathcal{T}_h)$ the L^2-projection, we define the error estimators*

$$\widetilde{\eta}_H := |||\phi_{h/2} - \Pi_h\phi_{h/2}||| \quad \text{and} \quad \widetilde{\mu}_H := \|\varrho^{1/2}(\phi_{h/2} - \Pi_h\phi_{h/2})\|_{L^2(\Gamma)}. \tag{3.7}$$

Then, there holds

$$\widetilde{\mu}_H \le \mu_H \le \sqrt{2}\, C_3\, \eta_H \quad \text{and} \quad \eta_H \le \widetilde{\eta}_H \le C_4\, \sigma(\mathcal{T}_h)^{1/2}\, \widetilde{\mu}_H \tag{3.8}$$

with the constants $C_3, C_4 > 0$ from Lemma 3.1. In particular, $\widetilde{\mu}_H$ is always efficient.

Proof. From the best approximation property of the Galerkin projection, we infer

$$\eta_H = |||\phi_{h/2} - \phi_h||| = |||(1 - \mathbb{G}_h)\phi_{h/2}||| \le |||(1 - \Pi_h)\phi_{h/2}||| = \widetilde{\eta}_H.$$

An application of (3.2) proves $\widetilde{\eta}_H \le C_4\, \|(h/\varrho)^{1/2}\|_{L^\infty(\Gamma)}\, \widetilde{\mu}_H$. To dominate $\widetilde{\mu}_H$ by μ_H, note that Π_h is the $\mathcal{T}_h$-elementwise L^2-projection, whence $\|(1 - \Pi_h)\phi_{h/2}\|_{L^2(T_j)} \le \|(1 - \mathbb{G}_h)\phi_{h/2}\|_{L^2(T_j)}$ for all $T_j \in \mathcal{T}_h$. If we sum this estimate over all elements, we are led to

$$\widetilde{\mu}_H = \|\varrho^{1/2}(1 - \Pi_h)\phi_{h/2}\|_{L^2(\Gamma)} \le \|\varrho^{1/2}(1 - \mathbb{G}_h)\phi_{h/2}\|_{L^2(\Gamma)} = \mu_H$$

which concludes the proof. □

***Remark* 5.** Theorem 3.2 states equivalence of all introduced error estimators — namely, η_H, $\widetilde{\eta}_H$, μ_H, and $\widetilde{\mu}_H$ — in case of either $d = 2$ or isotropic mesh-refinement in case of $d = 3$. However, the numerical experiments below indicate that the critical estimate $\widetilde{\eta}_H \lesssim \widetilde{\mu}_H$ does even hold for anisotropic mesh-refinement and $d = 3$. We stress that Theorem 3.4 is stronger than Theorem 3.2 in the sense that Equation (3.8) implies (3.5). □

4. Implementational Aspects

4.1. Computation of Galerkin Solutions. The implementation of Symm's integral equation is done as follows: For a given triangulation $\mathcal{T}_h = \{T_1, \dots, T_N\}$ of Γ we use the set of characteristic functions $\mathcal{B}_h := \{\chi_{T_j} : T_j \in \mathcal{T}_h\}$ as a basis of $\mathcal{P}^0(\mathcal{T}_h)$. In the experiments below, we restrict to the case that each element $T \in \mathcal{T}_h$ is an affine boundary piece for $d = 2$ and an axis parallel rectangle for $d = 3$, respectively. The entries

$$\mathbf{A}_{jk} = \langle V\chi_{T_k}, \chi_{T_j}\rangle$$

of the Galerkin matrix $\mathbf{A} \in \mathbb{R}^{N\times N}_{sym}$ are then computed analytically [17]. The computation of the right-hand side $\mathbf{b} \in \mathbb{R}^N$ with $\mathbf{b}_j = \langle f, \chi_{T_j}\rangle$ is discussed for each experiment separately. We refer to Section 5 for details. The Galerkin solution $\phi_h \in \mathcal{P}^0(\mathcal{T}_h)$ then reads $\phi_h = \sum_{j=1}^N \mathbf{x}_j\chi_{T_j}$, where the coefficient vector $\mathbf{x} \in \mathbb{R}^N$ is the unique solution of the linear system $\mathbf{A}\mathbf{x} = \mathbf{b}$.

Algorithm 3.3 requires the computation of discrete solutions with respect to a given coarse mesh $\mathcal{T}_h = \{T_1, \dots, T_N\}$ and its uniform refinement $\mathcal{T}_{h/2} = \{T_1, \dots, T_n\}$, where $n = kN$ with $k = 2$ in case of $d = 2$ and $k = 4$ in case of $d = 3$. We denote variables corresponding to the coarse and the fine mesh with an index h or $h/2$, respectively. The solution $\phi_{h/2} \in \mathcal{P}^0(\mathcal{T}_{h/2})$ is then obtained by solving the linear system $\mathbf{A}_{h/2}\mathbf{x}_{h/2} = \mathbf{b}_{h/2}$ as described above. In principle, the solution $\phi_h \in \mathcal{P}^0(\mathcal{T}_h)$ can be obtained by solving $\mathbf{A}_h\mathbf{x}_h = \mathbf{b}_h$. This naive approach,

however, needs the assembly of $\mathbf{A}_h$ and $\mathbf{b}_h$, which one aims to avoid for obvious reasons. Since iterative solvers like CG or GMRES only require a function for the matrix-vector multiplication with $\mathbf{A}_h$, we aim to provide this by use of the already computed matrix $\mathbf{A}_{h/2}$. To that end, note that each basis function $\chi_{T_j} \in \mathcal{B}_h$ of $\mathcal{P}^0(\mathcal{T}_h)$ may be written as a uniquely determined sum of functions in $\mathcal{B}_{h/2}$, e.g. $\chi_{T_j} = \chi_{T_{j_1}} + \chi_{T_{j_2}} + \chi_{T_{j_3}} + \chi_{T_{j_4}}$ for $d = 3$, cf. Figure 1. We define the prolongation operator $\mathbf{P}_h : \mathbb{R}^N \to \mathbb{R}^n$ which maps the coefficient vector $\mathbf{v}_h \in \mathbb{R}^N$ of a discrete function $v_h \in \mathcal{P}^0(\mathcal{T}_h)$ with respect to the basis $\mathcal{B}_h$ to the coefficient vector $\mathbf{v}_{h/2} = \mathbf{P}_h \mathbf{v}_h \in \mathbb{R}^n$ with respect to $\mathcal{B}_{h/2}$. We then compute the matrix-vector product $\mathbf{A}_h \mathbf{v}_h$ in the following way:

- Compute the prolongation $\mathbf{P}_h \mathbf{v}_h \in \mathbb{R}^n$.
- Compute the matrix-vector product $\mathbf{A}_{h/2} \mathbf{P}_h \mathbf{v}_h \in \mathbb{R}^n$.
- Compute $\mathbf{A}_h \mathbf{v}_h \in \mathbb{R}^N$ by summing up $(\mathbf{A}_h \mathbf{v}_h)_j = (\mathbf{A}_{h/2} \mathbf{P}_h \mathbf{v}_h)_{j_1} + \ldots + (\mathbf{A}_{h/2} \mathbf{P}_h \mathbf{v}_h)_{j_k}$ with $\chi_{T_j} = \chi_{T_{j_1}} + \ldots + \chi_{T_{j_k}}$.

By use of a Krylov-type solver one may thus obtain the Galerkin solution $\phi_h \in \mathcal{P}^0(\mathcal{T}_h)$ without computing and storing the corresponding matrix $\mathbf{A}_h \in \mathbb{R}^{N \times N}_{sym}$ explicitly. The same idea applies for the right-hand side $\mathbf{b}_h \in \mathbb{R}^N$ which can be computed on-the-fly:

- Compute $\mathbf{b}_h \in \mathbb{R}^N$ by summing up $(\mathbf{b}_h)_j = \langle f, \chi_{T_j} \rangle = (\mathbf{b}_{h/2})_{j_1} + \cdots + (\mathbf{b}_{h/2})_{j_k}$ with $\chi_{T_j} = \chi_{T_{j_1}} + \ldots + \chi_{T_{j_k}}$.

In this way, only $\mathbf{A}_{h/2}$ and $\mathbf{b}_{h/2}$ have to be computed and stored, which lowers the computational effort as well as the storage requirements significantly.

***Remark* 6.** If one uses matrix compression techniques like $\mathcal{H}$-matrices [2] and adaptive cross approximation [1], we found that it is a matter of stability to proceed in the aforegoing way to compute ϕ_h by use of $\mathbf{A}_{h/2}$ instead of $\mathbf{A}_h$. Compression techniques often use domain decompositions according to the geometry of a given mesh and try to store blocks of the matrix in a sparse way. Approximation errors in $\mathbf{A}_h$ and $\mathbf{A}_{h/2}$ stemming from this compression may thus correspond to different blocks of the matrices leading to artificially large deviances between ϕ_h and $\phi_{h/2}$ on certain boundary elements. In contrast to that, using $\mathbf{A}_{h/2}$ to compute ϕ_h, we observed that the compression error seems to have only minor influence on the difference $\phi_{h/2} - \phi_h$. □

4.2. Computation of Error Estimators. First, the error estimator η_H is simply computed by the Galerkin orthogonality

$$\eta_H^2 = |||\phi_{h/2} - \phi_h|||^2 = |||\phi_{h/2}|||^2 - |||\phi_h|||^2, \tag{4.1}$$

where both discrete energies are byproducts of the computation: The coefficient vector $\mathbf{x} \in \mathbb{R}^n$ of a Galerkin solution ϕ_h solves the Galerkin system $\mathbf{A}\mathbf{x} = \mathbf{b}$, so that the corresponding energy reads $|||\phi_h|||^2 = \mathbf{x} \cdot \mathbf{A}\mathbf{x} = \mathbf{x} \cdot \mathbf{b}$.

To compute $\widetilde{\eta}_H$, note that the L^2-projection Π_h onto $\mathcal{P}^0(\mathcal{T}_h)$ reads

$$(\Pi_h v)|_T = \frac{1}{|T|} \int_T v \, ds \quad \text{for all } v \in L^2(\Gamma) \text{ and } T \in \mathcal{T}_h, \tag{4.2}$$

where $|T|$ denotes the surface measure of $T \in \mathcal{T}_h$. Let $\mathbf{x}_{h/2}$ denote the coefficient vector of the Galerkin solution $\phi_{h/2} \in \mathcal{P}^0(\mathcal{T}_{h/2})$. Then the coefficient vector $\widetilde{\mathbf{x}}_h$ of the L^2-projection of

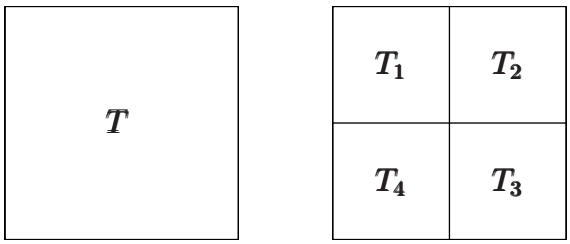

FIGURE 1. For the first implementation of Algorithm 3.3, a marked element T is always refined uniformly into 4 new elements T_j. This isotropic refinement obviously yields $h_j = h/2$ and $\varrho_j = \varrho/2$ for the refined mesh-sizes.

$\phi_{h/2}$ onto $\mathcal{P}^0(\mathcal{T}_h)$ may be simply computed as

$$(\widetilde{\mathbf{x}}_h)_j = (\mathbf{x}_{h/2,j_1} + \ldots + \mathbf{x}_{h/2,j_k})/k. \tag{4.3}$$

This follows from $\mathcal{T}_{h/2}$ being the uniform refinement of $\mathcal{T}_h$, so that there holds $|T_{j_\ell}| = |T_j|/k$ for $\ell = 1, \ldots, k$ with $k = 2, 4$ for $d = 2, 3$, respectively. The computation of $\widetilde{\eta}_H$ thus reads

$$\widetilde{\eta}_H^2 = \|\!|\phi_{h/2} - \Pi_h \phi_{h/2}|\!\|^2 = (\mathbf{x}_{h/2} - \mathbf{P}_h \widetilde{\mathbf{x}}_h) \cdot \mathbf{A}_{h/2}(\mathbf{x}_{h/2} - \mathbf{P}_h \widetilde{\mathbf{x}}_h), \tag{4.4}$$

where $\mathbf{P}_h$ again denotes the prolongation operator from Section 4.1.

The estimators $\mu_H = \|\varrho^{1/2}(\phi_{h/2} - \phi_h)\|_{L^2(\Gamma)}$ and $\widetilde{\mu}_H = \|\varrho^{1/2}(\phi_{h/2} - \Pi_h \phi_{h/2})\|_{L^2(\Gamma)}$ are computable from the already assembled data. Note, that the implementation of a mesh-size weighted L^2-norm for piecewise polynomials is fairly standard and can be performed analytically without any additional quadrature error.

In particular, we stress that the computational complexity of the estimators $\widetilde{\eta}_H$, $\widetilde{\mu}_H$ and μ_H is negligible compared to the cost for the computation of the Galerkin solution ϕ_h resp. $\phi_{h/2}$.

4.3. Mesh-Refinement in 2D. In our 2D experiments, we restrict to the case that the boundary Γ is split into affine boundary pieces $\Gamma_1, \ldots, \Gamma_r$ and that the triangulation consists of flat boundary elements, i.e. line segments. In the experiments below, we choose a uniform initial mesh $\mathcal{T}_h^{(0)}$. For both, uniform and adaptive mesh-refinement, marked elements T are halved into two new elements T_1 and T_2 with $h_T = 2h_{T_1} = 2h_{T_2}$. For adaptive mesh-refinement, we use Algorithm 3.3 steered by the localized error estimator μ_H and the adaptivity parameter $\theta = 0.5$. In order to ensure a uniform upper bound for the K-mesh constant, we check the mesh-size ratio of neighbouring elements: If an element T_i is marked for refinement we additionally mark neighbouring elements T_j with

$$h_j/h_i \geq 2 \quad \text{and} \quad T_i \cap T_j \neq \emptyset. \tag{4.5}$$

This guarantees $\kappa(\mathcal{T}_h^{(\ell)}) \leq 2\kappa(\mathcal{T}_h^{(0)})$ for all adaptively generated meshes $\mathcal{T}_h^{(\ell)}$. We stress, that the K-mesh property is crucial for the estimates stated in Lemma 3.1, and thus the equivalency of the introduced error estimators.

4.4. Isotropic Mesh-Refinement in 3D. In our 3D experiments, we restrict to the case that the elements $T_j \in \mathcal{T}_h$ are axis parallel squares. For uniform and adaptive isotropic refinement, each marked element T_j is split into 4 new elements such that h_j as well as ϱ_j

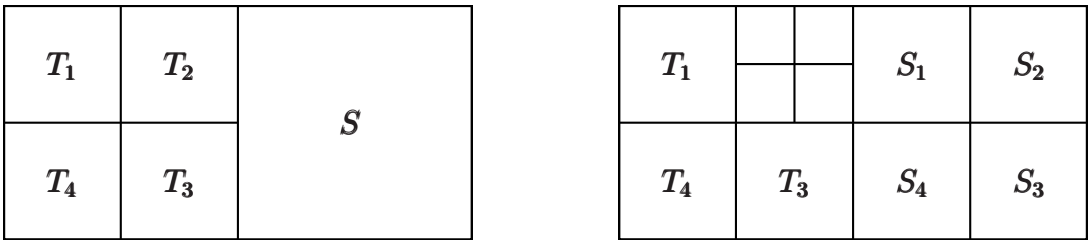

FIGURE 2. One hanging node per edge is allowed (left). If, in the left configuration, element T_2 is marked for refinement, we mark element S for refinement as well (right).

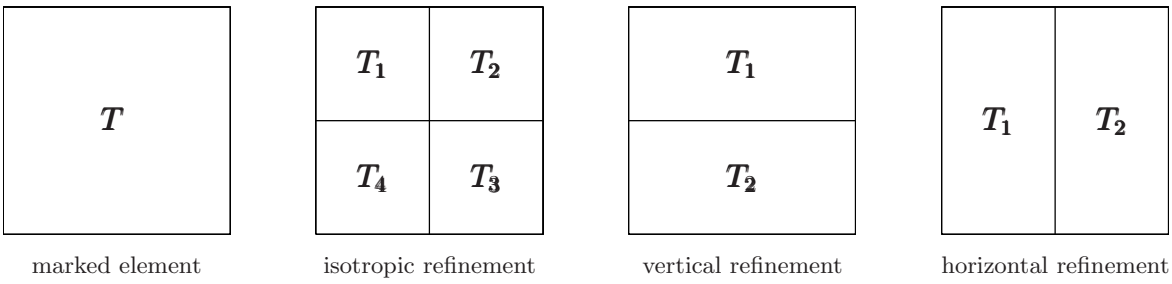

FIGURE 3. The modification of Algorithm 3.3 gives a criterion whether a marked rectangle $T \in \mathcal{T}_h$ (left) is refined isotropically into four elements $T_1, \ldots, T_4$ or anisotropically into two elements T_1 and T_2. In the latter case, the algorithm decides whether vertical or horizontal refinement seems to be more appropriate.

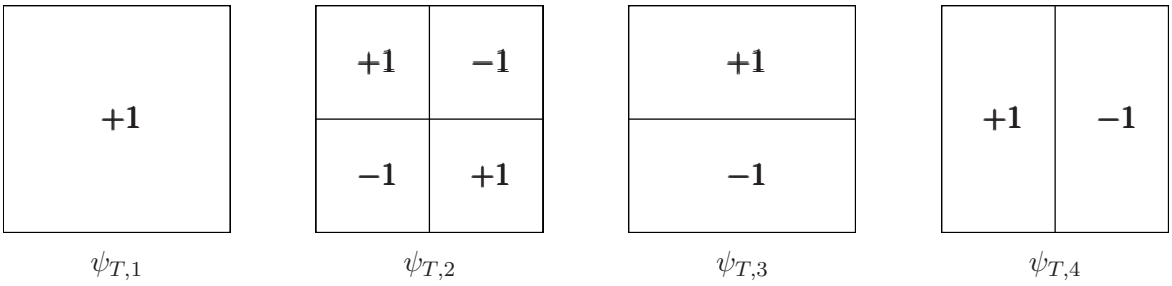

FIGURE 4. For each rectangle $T \in \mathcal{T}_h$, we introduce four $\mathcal{T}_{h/2}$-piecewise constant functions $\psi_{T,j} \in \mathcal{P}^0(\mathcal{T}_{h/2})$, which are extended by zero to $\Gamma \backslash T$.

are halved, cf. Figure 1. We stress that, due to the initial mesh and this mesh-refinement rule, the mesh-widths $\varrho = h$ coincide. For adaptive isotropic mesh-refinement, we again use Algorithm 3.3 with $\theta = 0.5$ and μ_H for marking. To ensure the K-mesh property of the triangulations, we only allow one hanging node per edge, cf. Figure 2. Note, that this

restriction automatically ensures $\varrho_i/\varrho_j = h_i/h_j \leq 2$ for neighbouring elements T_i, T_j which share an edge.

4.5. Anisotropic Mesh-Refinement in 3D. The 3D experiments in Section 5.4–5.5 show that the experimental order of convergence is improved in the case of isotropic mesh-refinement when compared to the order of convergence for uniform mesh-refinement. However, the isotropic refinement strategy does not reveal the optimal order of convergence. To overcome this gap, we extend Algorithm 3.3 to allow anisotropic mesh-refinement. More precisely, we extend step (vi) of Algorithm 3.3 by a heuristic criterion to decide whether a marked rectangle $T \in \mathcal{T}_h$ is refined into 2 or 4 rectangles, cf. Figure 3. To that end, we use that we have already computed $\phi_{h/2}$. Let $T_1, \dots, T_4 \in \mathcal{T}_{h/2}$ denote the four son-elements of a marked coarse-mesh element $T \in \mathcal{T}_h$, where we use the same numbering as for the isotropic refinement of Figure 3. Now, consider the four piecewise constant functions $\psi_{T,j} \in \mathcal{P}^0(\mathcal{T}_{h/2})$ from Figure 4 and observe that $\{\psi_{T,1}, \dots, \psi_{T,4}\}$ is an L^2-orthogonal basis of $\mathcal{P}^0(\{T_1, \dots, T_4\})$. Therefore, $\phi_{h/2}|_T \in \mathcal{P}^0(\{T_1, \dots, T_4\})$ reads

$$\phi_{h/2}|_T = \sum_{j=1}^{4} c_{T,j}\psi_{T,j} \quad \text{with the Fourier coefficients} \quad c_{T,j} = \frac{(\psi_{T,j}\,, \phi_{h/2})_{L^2(T)}}{\|\psi_{T,j}\|^2_{L^2(T)}}. \tag{4.6}$$

The decision whether isotropic or anisotropic refinement is more appropriate, is now done as follows. We assume that $T \in \mathcal{T}_h$ is marked for refinement:

- If $c_{T,3}$ is significantly larger than the Fourier coefficients $c_{T,2}$ and $c_{T,4}$ the discrete solution $\phi_{h/2}|_T$ is rather constant in the horizontal direction. Therefore, the vertical refinement from Figure 3 seems to be more efficient than isotropic refinement.
- If $c_{T,4}$ is significantly larger than the Fourier coefficients $c_{T,2}$ and $c_{T,3}$, the discrete solution $\phi_{h/2}|_T$ is rather constant in the vertical direction. Therefore, the horizontal refinement from Figure 3 seems to be more efficient than isotropic refinement.
- Otherwise, we do isotropic refinement.

Here, significantly larger is understood in the following sense: Let $\tau \in (0, 1)$ be a fixed parameter. Then, $c_{T,3}$, for instance, is significantly larger than $c_{T,2}$ and $c_{T,4}$, provided that

$$\tau|c_{T,3}| \geq \big(|c_{T,2}|^2 + |c_{T,4}|^2\big)^{1/2}. \tag{4.7}$$

For the numerical experiments below, we choose $\tau = 0.5$.

Note, that the Fourier coefficients are easy to compute. Since we use characteristic basis functions, our computations provide the coefficients $\lambda_{T,1}, \dots, \lambda_{T,4} \in \mathbb{R}$ such that

$$\phi_{h/2}|_T = \sum_{k=1}^{4} \lambda_{T,k}\chi_{T_k},$$

where $T_1, \dots, T_4 \in \mathcal{T}_{h/2}$ are the sons of $T \in \mathcal{T}_h$ as in Figure 3. We then observe

$$\|\psi_{T_j}\|^2_{L^2(T)} = |T| \quad \text{as well as} \quad (\psi_{T,j}\,, \phi_{h/2})_{L^2(T)} = \sum_{k=1}^{4} \lambda_{T,k} \int_{T_k} \psi_{T,j}\, dx.$$

Note that the integral has the value $\pm|T|/4$ according to the definition of the functions $\psi_{T,j}$. A comparison of Figure 3 and 4 now shows that

$$\begin{pmatrix} c_{T,1} \\ c_{T,2} \\ c_{T,3} \\ c_{T,4} \end{pmatrix} = \frac{1}{4} \begin{pmatrix} 1 & 1 & 1 & 1 \\ 1 & -1 & 1 & -1 \\ 1 & 1 & -1 & -1 \\ 1 & -1 & -1 & 1 \end{pmatrix} \begin{pmatrix} \lambda_{T,1} \\ \lambda_{T,2} \\ \lambda_{T,3} \\ \lambda_{T,4} \end{pmatrix},$$

where we simply plugged-in the values $\psi_{T,j}|_{T_k}$.

As in the isotropic case, we restrict to one hanging node per edge. This, however, does not ensure, that the K-mesh constant $\kappa(\mathcal{T}_h)$ stays uniformly bounded, since the local mesh-size ϱ may vary arbitrarily between neighbouring elements due to the anisotropic refinements. In our implementation, we therefore do some additional marking, where we check the aspect ratio ϱ_i/ϱ_j for neighbouring elements: Let T_i be marked and let T_j share an edge with T_i. If $\varrho_j/\varrho_i \geq 2$, we also mark T_j for refinement. Together with the uniform initial mesh $\mathcal{T}_h^{(0)}$, this ensures that ϱ and h may only vary by a factor 2 on neighbouring elements.

5. Numerical Experiments

This section reports on three numerical experiments to study the accuracy of the introduced error estimators and the performance of the proposed adaptive strategy. Example 5.3 considers Symm's integral equation in 2D corresponding to a Dirichlet problem on the L-shaped domain with reentrant corner at the origin. The exact solution of the PDE is given in polar coordinates by $u(r,\varphi) = r^\alpha \cos(\alpha\varphi)$ and has a generic singularity with $\alpha = 2/3$ at the reentrant corner $(0,0)$, where the interior angle is $3\pi/2$.

In Example 5.4–5.5, we study the performance of the proposed method for Symm's integral equation in 3D. For the ease of implementation and to exclude any positive or negative effects of numerical quadrature, we consider

$$V\phi = 1 \quad \text{on } \Gamma, \tag{5.1}$$

for Γ being the L-shaped screen in Example 5.4 and the surface $\Gamma = \partial\Omega$ of the Fichera cube $\Omega = (-1,1)^3 \backslash [0,1]^3$ in Example 5.5. In both cases, the solution ϕ appears to be singular so that uniform mesh-refinement leads to a suboptimal order of convergence for the error $|||\phi - \phi_h|||$.

All adaptive experiments are performed by use of Algorithm 3.3, where we choose $\theta = 0.5$ to steer the mesh-refinement. For the marking step (v) in Algorithm 3.3, we use the local contributions

$$\mu_{H,j}^2 = \varrho_j \|\phi_{h/2} - \phi_h\|_{L^2(T_j)}^2$$

of μ_H. Anisotropic mesh-refinement in 3D is obtained by the extended Algorithm described in Section 4.5, where we use $\theta = 0.5$ for marking and $\tau = 0.5$ for the decision which kind of refinement is chosen, cf. Figure 3. To control the K-mesh property of the adaptively generated meshes $\mathcal{T}_h^{(\ell)}$, we perform some additional marking as described in Sections 4.3–4.5.

5.1. Visualization and Interpretation of Numerical Results. The error in the energy norm is computed by use of the Galerkin orthogonality

$$|||\phi - \phi_h||| = \big(|||\phi|||^2 - |||\phi_h|||^2\big)^{1/2}. \tag{5.2}$$

We obtained $|||\phi|||^2$ with the help of Aitkin's Δ^2-method, where we extrapolated the energies $|||\phi_h^{(\ell)}|||^2$ for a sequence of discrete solutions on uniform meshes $\mathcal{T}_h^{(\ell)}$. Besides the error, we compute the four introduced error estimators

$$\eta_H = |||\phi_{h/2} - \phi_h|||, \qquad \mu_H = \|\varrho^{1/2}(\phi_{h/2} - \phi_h)\|_{L^2(\Gamma)},$$
$$\widetilde{\eta}_H = |||\phi_{h/2} - \Pi_h\phi_{h/2}|||, \qquad \widetilde{\mu}_H = \|\varrho^{1/2}(\phi_{h/2} - \Pi_h\phi_{h/2})\|_{L^2(\Gamma)}.$$

In Figure 7, 10, 11, 14, and 15, we then plot the Galerkin error $|||\phi - \phi_h|||$ as well as the four error estimators against the number $N = \#\mathcal{T}_h$ of elements, where both axes are scaled logarithmically. In the double-logarithmic plot, an experimental convergence order $\mathcal{O}(N^{-\alpha})$ is visible in the slope $-\alpha$ of a straight curve. Note that, for uniform mesh-refinement, the order $\mathcal{O}(N^{-\alpha})$ with respect to the number N of elements corresponds to the order $\mathcal{O}(h^\alpha)$ in two dimensions and to $\mathcal{O}(h^{2\alpha})$ in three dimensions with respect to the uniform mesh-size h.

We recall that for piecewise constant ansatz functions, the optimal order of convergence is $\alpha = 3/2$ and $\alpha = 3/4$ for $d = 2, 3$, respectively, cf. [19]. However, this order is usually spoiled by lack of regularity of the exact solution $\phi \in \widetilde{H}^{-1/2}(\Gamma)$ and not observed for uniform mesh-refinement. We thus aim to regain this optimal order experimentally by use of adaptive mesh-refinement.

From our analysis, we know that η_H is always efficient with constant $C_{\text{eff}} = 1$. Therefore, the absolute values and hence the curve of the error estimator η_H should be below the error. In all experiments, we observe that the curves of the error and η_H are even parallel. This empirically proves reliability of η_H, which is equivalent to the saturation assumption (A), cf. Proposition 1.1. For 2D and isotropic mesh-refinement in 3D, Theorem 3.4 states the equivalency of the four error estimators, namely there hold the inequalities

$$\eta_H \le \widetilde{\eta}_H \lesssim \widetilde{\mu}_H \le \mu_H \lesssim \eta_H,$$

whose implications are threefold: First, the curve corresponding to η_H should always be below the curve of $\widetilde{\eta}_H$. Second, the curve corresponding to $\widetilde{\mu}_H$ should always be below the curve of μ_H. Finally, all of the four curves of the error estimators should be parallel in a certain range. We stress, that our analysis only provides equivalency of all introduced error estimators in the case, that the shape-regularity $\sigma(\mathcal{T}_h^{(\ell)})$ stays uniformly bounded as $\ell \to \infty$. In particular our results do not cover adaptive anisotropic mesh-refinements in 3D. However, we observe that even in the latter case the curves of the error estimators are (up to a certain range) parallel. This gives empirical evidence that the factor $\sigma(\mathcal{T}_h)^{1/2}$ in (3.5) resp. (3.8) is too pessimistic and can be dropped.

For all refinement strategies, we observe that $\eta_H \approx \widetilde{\eta}_H$ and $\mu_H \approx \widetilde{\mu}_H$ in the sense that the curves almost coincide. For optimal mesh-refinement, i.e. adaptive refinement in 2D and anisotropic adaptive refinement in 3D, we see furthermore that the error $|||\phi - \phi_h|||$ is accurately estimated by η_H. To exploit these observations in more detail, Figure 8 and 12 provide the experimental constants C_{rel}, C_η, and C_μ for the three estimates

$$\eta_H \le |||\phi - \phi_h||| \le C_{\text{rel}}\,\eta_H, \quad \eta_H \le \widetilde{\eta}_H \le C_\eta^{-1}\,\eta_H, \quad \widetilde{\mu}_H \le \mu_H \le C_\mu^{-1}\,\widetilde{\mu}_H. \tag{5.3}$$

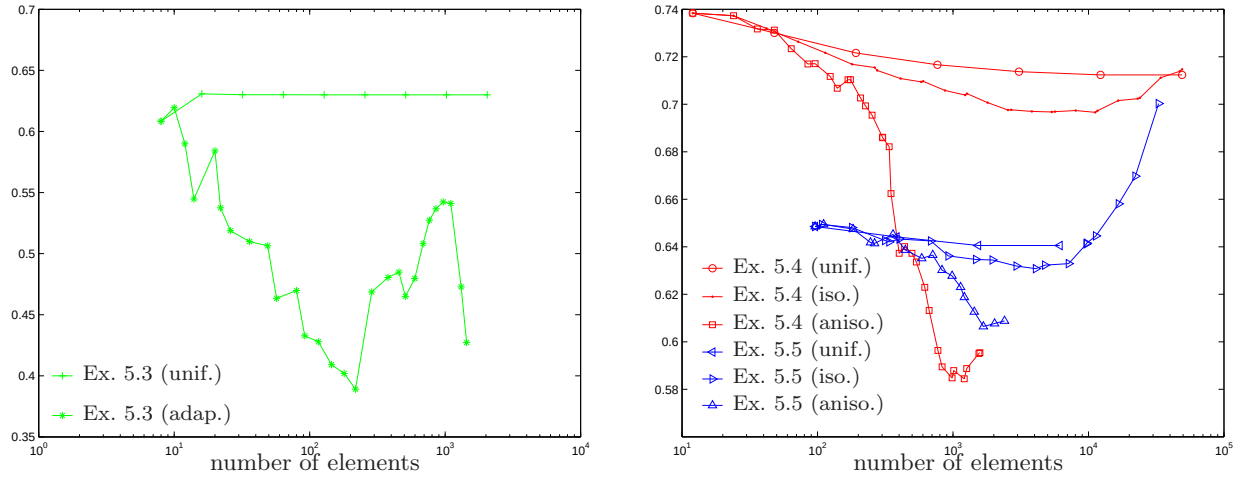

FIGURE 5. Experimental saturation constant $C_{\mathrm{sat}} = |||\phi - \phi_{h/2}|||/|||\phi - \phi_h|||$ for uniform as well as μ_H-adaptive (isotropic and anisotropic) mesh-refinement. In any case holds $C_{\mathrm{sat}} \leq 0.65$ in 2D and $C_{\mathrm{sat}} \leq 0.75$ in 3D, which yields reliability of η_H.

For the two 3D experiments, Figure 9 and 13 show adaptively generated meshes, from which edge singularities of the exact solution are visible. Finally, Figure 16 plots the error over the corresponding computational time. We observe that, even from this practical point of view, adaptive mesh-refinement is superior to uniform mesh-refinement.

5.2. Remarks on the Saturation Assumption. Reliability of η_H holds under the saturation assumption, which then implies that the error curve is parallel to the curve of η_H. In Figure 5, we thus plot the experimental saturation constant $C_{\mathrm{sat}} = |||\phi - \phi_{h/2}|||/|||\phi - \phi_h|||$ and observe $C_{\mathrm{sat}} < 0.65$ in $2D$ and $C_{\mathrm{sat}} < 0.75$ uniformly for both, uniform and adaptive mesh-refinement. This gives empirical evidence that the saturation assumption (A) holds.

Under some additional regularity assumptions on the exact solution ϕ, a numerical scheme usually leads to some convergence order $|||\phi - \phi_h||| = \mathcal{O}(N^{-\alpha})$ for some $\alpha > 0$. We suppose that we are in an asymptotic regime and use the ansatz

$$|||\phi - \phi_h||| = CN^{-\alpha} \quad \text{as well as} \quad |||\phi - \phi_{h/2}||| = C(kN)^{-\alpha}$$

with $k = 2, 4$ for $d = 2, 3$, respectively. Under this assumption and in an asymptotic sense, the saturation constant then satisfies

$$C_{\mathrm{sat}} = \frac{|||\phi - \phi_{h/2}|||}{|||\phi - \phi_h|||} = k^{-\alpha} < 1.$$

For 2D and if the (adaptive) algorithm reveals the optimal order of convergence $\alpha = 3/2$, this asymptotically predicts

$$C_{\mathrm{sat}} = 2^{-3/2} \approx 0.3536 \quad \text{as well as} \quad C_{\mathrm{rel}} = (1 - C_{\mathrm{sat}}^2)^{-1/2} \approx 1.0690,$$

cf. Proposition 1.1. The same holds for 3D, where $k = 4$ and $\alpha = 3/4$ in case of optimal order of convergence, i.e., $C_{\mathrm{sat}} = 4^{-3/4} = 2^{-3/2}$.

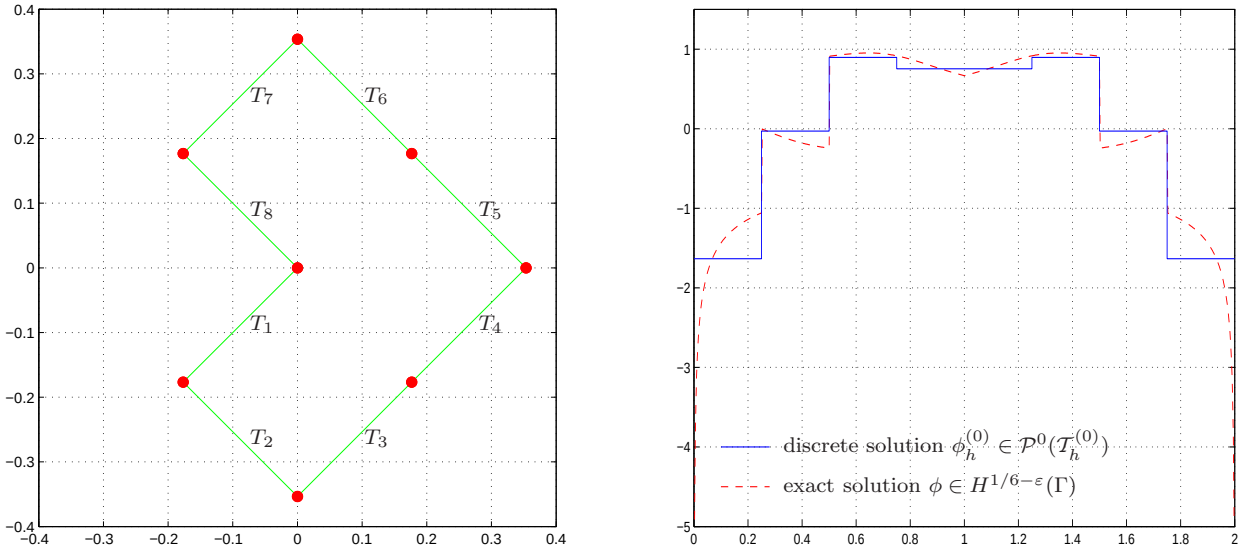

FIGURE 6. Initial mesh $\mathcal{T}_h^{(0)}$ with $N = 8$ elements (left) in Example 5.3 and corresponding discrete solution $\phi_h^{(0)} \in \mathcal{P}^0(\mathcal{T}_h^{(0)})$ plotted over the arc-length s (right), where $s(0) = s(2)$ corresponds to the reentrant corner $(0, 0) \in \Gamma$. For comparison, the right figure even shows the exact solution $\phi \in H^{1/6-\varepsilon}(\Gamma)$.

5.3. Symm's Integral Equation for Dirichlet Problem in 2D. We consider the Dirichlet problem

$$-\Delta u = 0 \quad \text{in } \Omega \quad \text{with boundary conditions} \quad u = g \quad \text{on } \Gamma := \partial\Omega \tag{5.4}$$

on the L-shaped domain $\Omega \subset \mathbb{R}^2$ shown in Figure 6 with known exact solution

$$u(x) = r^\alpha \cos(\alpha\varphi) \quad \text{in polar coordinates} \quad x = r\,(\cos\varphi, \sin\varphi) \tag{5.5}$$

for some fixed parameter $\alpha > 0$. With the simple-layer potential V from (1.2) and the double-layer potential K defined by

$$K : H^{1/2}(\Gamma) \to H^{1/2}(\Gamma), \quad Kv(x) = \int\!\!\!\!\!\!-_\Gamma v(y) \frac{\partial}{\partial n_y} G(x - y)\, ds_y, \tag{5.6}$$

Symm's integral equation

$$V\phi = (1/2 + K)g \tag{5.7}$$

is an equivalent formulation of the Dirichlet problem (5.5), cf. [18]. The unique solution $\phi \in H^{-1/2}(\Gamma)$ of (5.7) is the normal derivative $\phi = \partial u/\partial n$, which reads in polar coordinates

$$\phi(x) = (w \cdot n(x))\, \alpha r^{\alpha-1} \quad \text{with } w := \begin{pmatrix} \cos(\varphi)\cos(\alpha\varphi) + \sin(\varphi)\sin(\alpha\varphi) \\ \sin(\varphi)\cos(\alpha\varphi) - \cos(\varphi)\sin(\alpha\varphi) \end{pmatrix} \in \mathbb{R}^2. \tag{5.8}$$

For the numerical experiment, we choose $\alpha = 2/3$. The Dirichlet problem then leads to $u \notin H^2(\Omega)$ with a generic singularity at the reentrant corner.

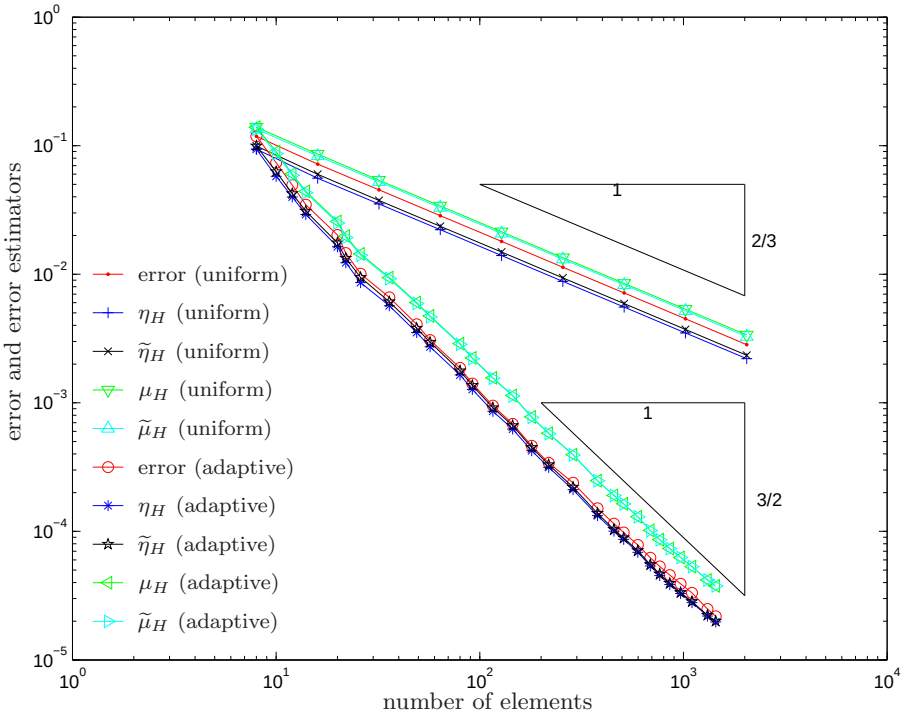

FIGURE 7. Error $|||\phi - \phi_h|||$ and error estimators η_H, $\widetilde{\eta}_H$, μ_H, $\widetilde{\mu}_H$ in Dirichlet Problem 5.3 on L-shaped domain for uniform and μ_H-adaptive mesh-refinement.

To compute the entries of the right-hand side $\mathbf{b} \in \mathbb{R}^N$ for the Galerkin scheme, we use the adjoint double-layer potential K' and write

$$\mathbf{b}_j = \langle (1/2 + K)g\,, \chi_{T_j} \rangle = \langle g\,, (1/2 + K')\chi_{T_j} \rangle = \frac{1}{2} \int_{T_j} g\, ds + \sum_{k=1}^{N} \int_{T_k} g(x) K' \chi_{T_j}(x)\, ds_x.$$

The first integral is computed by Gauss quadrature. Although $\texttt{adlp}(T_j; x) := (K^* \chi_{T_j})(x)$ can be computed via an analytic formula, it leads to weak singularities for x near T_j. For a neighbouring element T_k, we thus use an explicit decomposition

$$\texttt{adlp}(T_j; x) = a\, \log(|x - b|/|x - c|) + \text{smooth}(x)$$

for some parameters a, b, and c to obtain

$$\int_{T_k} g(x)\, \texttt{adlp}(T_j; x)\, ds_x = \int_0^1 g(\gamma(s))\, \log s\, ds + \int_{T_k} g(x)\, \text{smooth}(x)\, ds_x.$$

The first integral is computed with a weighted Gauss quadrature rule, whereas the other integral involves a smooth integrand and is hence approximated by simple Gauss quadrature. Throughout, we found that the use of quadrature rules of order 7 was sufficient.

The initial coarse mesh $\mathcal{T}_h^{(0)}$ with $N = 8$ equisized elements and the corresponding discrete solution $\phi_h^{(0)} \in \mathcal{P}^0(\mathcal{T}_h^{(0)})$ as well as the exact solution are visualized in Figure 6. Here, ϕ and $\phi_h^{(0)}$ are shown as plots over the arc-length. The singularity of ϕ at $(0, 0)$ is visible at

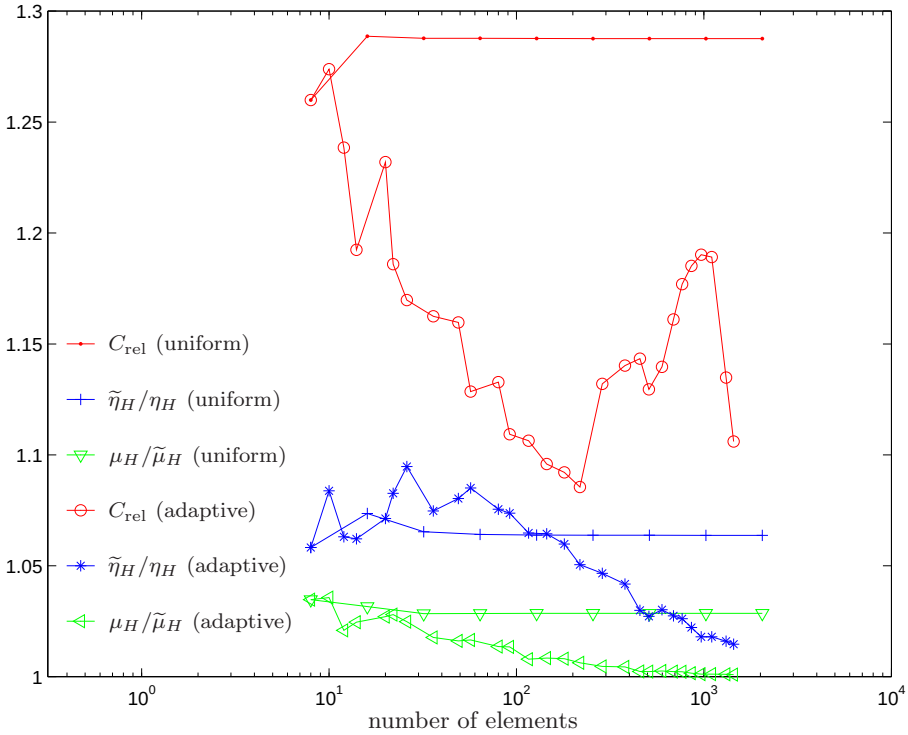

FIGURE 8. Experimental reliability constant $C_{\rm rel} = |||\phi - \phi_h|||/\eta_H$ as well as quotients $C_\eta = \widetilde{\eta}_H/\eta_H$ and $C_\mu = \mu_H/\widetilde{\mu}_H$ in Dirichlet Problem 5.3 for uniform and μ_H-adaptive mesh-refinement.

arc-length parameter $s = 0$ and $s = 2$ by periodicity. We computed the Galerkin error by use of the extrapolated value $|||\phi|||^2 = 0.4041161973$ in (5.2).

Figure 7 provides the curves of the error and the four error estimators for both, uniform and adaptive mesh-refinement. As can be predicted from theory, we observe a suboptimal order of convergence $|||\phi - \phi_h||| = \mathcal{O}(N^{-2/3})$ for the error for uniform mesh-refinement. Moreover, all five curves are parallel, which empirically proves reliability and efficiency of all error estimators.

The adaptively generated meshes show a strong refinement towards the reentrant corner, and the adaptive mesh-refinement leads to the optimal order of convergence $|||\phi - \phi_h||| = \mathcal{O}(N^{-3/2})$. As for uniform mesh-refinement, we observe reliability and efficiency of all error estimators in the sense that the corresponding curves are parallel.

In Figure 8, we see that the reliability constant satisfies $C_{\rm rel} \approx 1.29$ for uniform mesh-refinement, where the asymptotic ansatz from Section 5.2 predicts $C_{\rm rel} \approx 1.2876$ for $\alpha = 2/3$. Moreover, $C_{\rm rel}$ is even improved by adaptive mesh-refinement. For the experimental constants defined in (5.3), we observe $C_\eta \approx 1.06$ and $C_\mu \approx 1.03$ for uniform mesh-refinement, where both constants tend to 1 for adaptive mesh-refinement.

5.4. Symm's Integral Equation on L-Shaped Screen in 3D. We consider Symm's integral equation (5.1) on the L-shaped screen Γ, which is visualized together with some adaptively generated meshes in Figure 9. The exact solution ϕ is unknown, but discrete solutions show certain singularities along the edges and at the five convex corners of Γ.

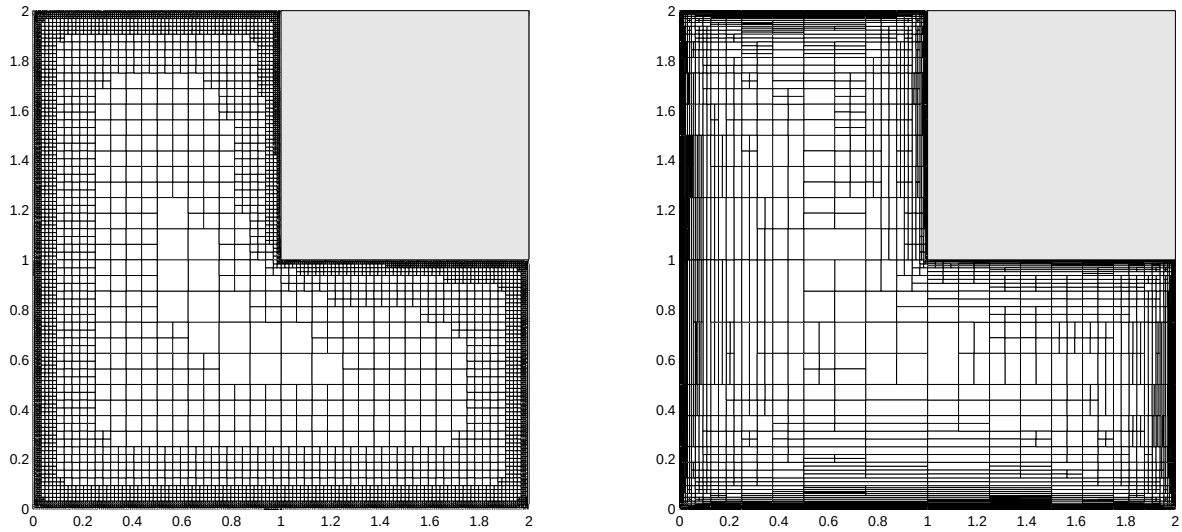

FIGURE 9. Adaptively generated isotropic mesh $\mathcal{T}_h^{(29)}$ with $N = 49.116$ elements (left) in Screen Problem 5.4 as well as adaptively generated anisotropic mesh $\mathcal{T}_h^{(37)}$ with $N = 3.313$ elements (right). The initial mesh $\mathcal{T}_h^{(0)}$ consisted of $N = 12$ squares with uniform mesh-size $h = \varrho = 1/2$. We observe mesh-refinement along all edges of Γ.

To compute the energy error, we use the extrapolated value $|||\phi|||^2 = 8.28466$ in (5.2). Error and error estimators for uniform and isotropic mesh-refinement are plotted in Figure 10. As predicted by theory, all error estimators are efficient, and the corresponding curves are parallel. Moreover, for both mesh-refining strategies, uniform and isotropic adaptive, we obtain experimental reliability since the curve of the error $|||\phi - \phi_h|||$ is parallel to the curves of the corresponding error estimators.

With respect to the order of convergence, we observe that uniform refinement leads to a suboptimal order $\mathcal{O}(N^{-1/4})$. Isotropic mesh-refinement steered by μ_H and Algorithm 3.3 leads to an improved convergence order of almost $\mathcal{O}(N^{-1/2})$. However, the optimal order of convergence is $\mathcal{O}(N^{-3/4})$. One therefore should be able to resolve the singularities more effectively than isotropic refinements allow to.

Figure 11 shows the error and error estimators for uniform and anisotropic adaptive mesh-refinement, cf. Section 4.5. We observe that the optimal order of convergence $\mathcal{O}(N^{-3/4})$ is, in fact, revealed by the anisotropic strategy. Moreover, the curves of all error estimators are parallel in a certain range, which suggests that our analysis is too pessimistic and the factor $\sigma(\mathcal{T}_h)^{1/2}$ in (3.5) resp. (3.8) may be dropped.

Figure 9 shows the meshes $\mathcal{T}_h^{(29)}$ with $N = 49.116$ elements generated by μ_H-adaptive isotropic mesh-refinement and $\mathcal{T}_h^{(37)}$ with $N = 3.313$ elements obtained by μ_H-adaptive anisotropic mesh-refinement. We observe strong refinements towards all the edges and the convex corners. Obviously the anisotropic mesh resolves edge singularities more efficiently, that the isotropic mesh. Even though the solution ϕ seems to be smooth at the reentrant corner $(1, 1, 0)$, the algorithm leads to a local refinement to ensure the uniform boundedness of the K-mesh constant $\kappa(\mathcal{T}_h)$, cf. Section 4.5.

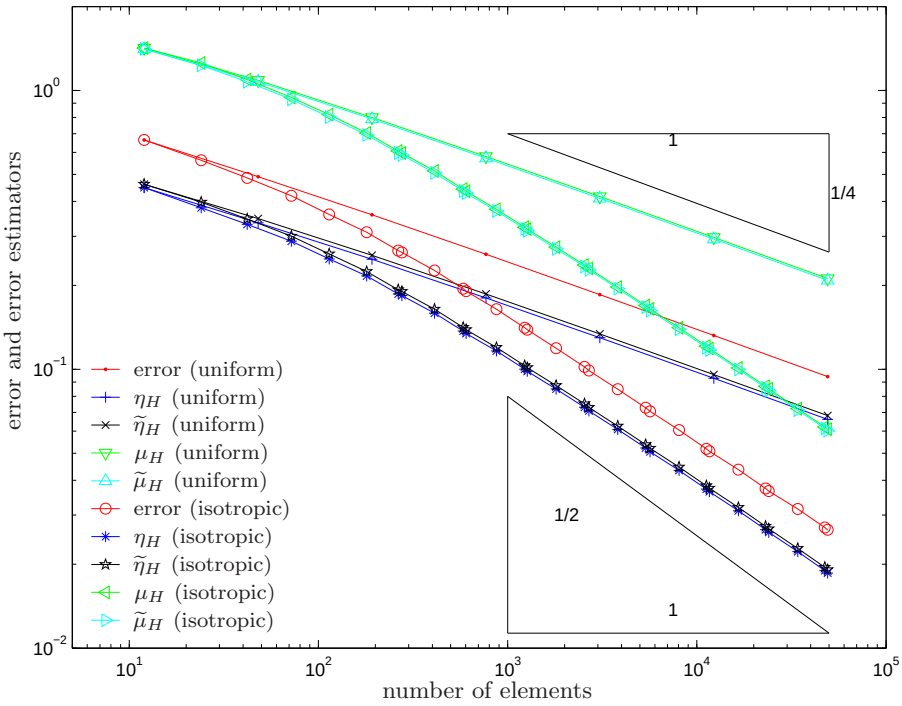

FIGURE 10. Error $|||\phi - \phi_h|||$ and error estimators $\eta_H, \widetilde{\eta}_H, \mu_H, \widetilde{\mu}_H$ in Screen Problem 5.4 for uniform and μ_H-adaptive isotropic mesh-refinement.

Considering the experimental constants $C_{\mathrm{rel}} = |||\phi - \phi_h|||/\eta_H$, $C_\eta = \widetilde{\eta}_H/\eta_H$, and $C_\mu = \mu_H/\widetilde{\mu}_H$ from (5.3), we observe that C_η and C_μ are not as close to 1 as in the 2D experiment. However, C_{rel} is improved in the anisotropic adaptive case, i.e., C_{rel} decreases with increasing number $N = \#\mathcal{T}_h$ of elements. This is also reflected by the fact, that the curve of η_H gets closer to the curve of the error $|||\phi - \phi_h|||$ with increasing N in Figure 11. Moreover, for adaptive anisotropic mesh-refinement, we see that C_η and C_μ seem to be even slightly increasing with N.

5.5. Capacity of Fichera's Cube in 3D. We consider Symm's integral equation (5.1) on the boundary Γ of the Fichera cube $\Omega = [-1,1]^3 \setminus [0,1]^3$. The boundary together with some adaptively generated meshes is shown in Figure 13. Even though the exact solution ϕ is unknown, theory predicts that generic singularities should arise along all edges for this capacity problem.

To compute the energy error, we use the extrapolated value $|||\phi|||^2 = 16.2265$ in (5.2). Error and error estimators for uniform and isotropic mesh-refinement are plotted in Figure 14. As predicted by theory, all error estimators are efficient, and the corresponding curves are even parallel. Moreover, we again obtain numerical evidence of reliability since the curve of the error $|||\phi - \phi_h|||$ is parallel to the curves of the corresponding error estimators.

With respect to the order of convergence, we observe a similar behaviour to the one obtained in Screen Problem 5.4: Uniform refinement leads to a suboptimal order $\mathcal{O}(N^{-1/4})$, isotropic mesh-refinement steered by μ_H and Algorithm 3.3 leads to an improved convergence order of almost $\mathcal{O}(N^{-1/2})$, cf. Figure 14. Adaptive anisotropic mesh-refinement again reveals the optimal order of convergence $\mathcal{O}(N^{-3/4})$, cf. Figure 15.

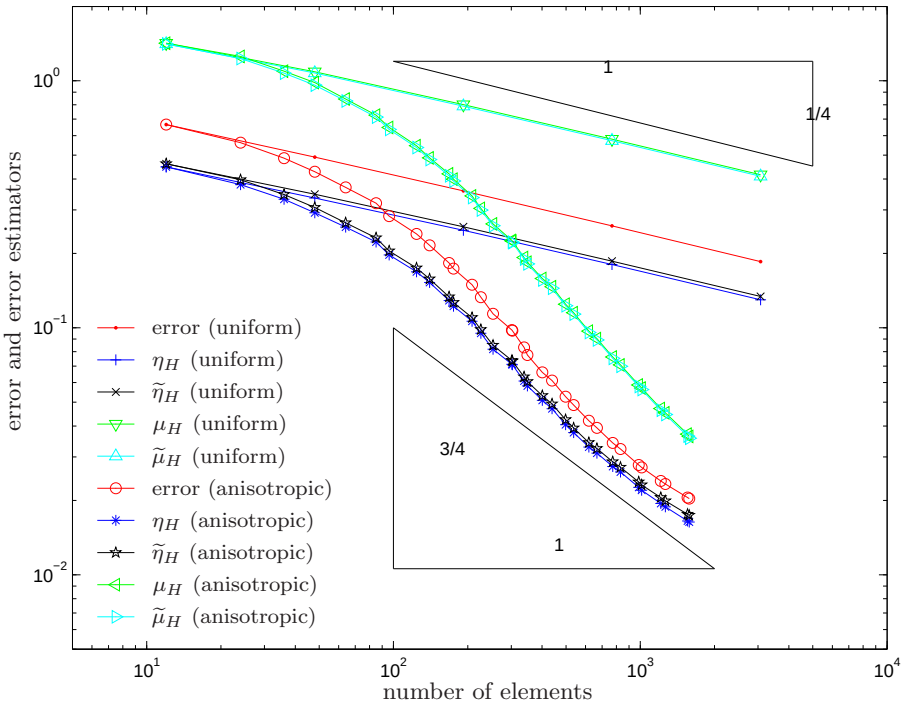

FIGURE 11. Error $|||\phi - \phi_h|||$ and error estimators $\eta_H, \widetilde{\eta}_H, \mu_H, \widetilde{\mu}_H$ in Screen Problem 5.4 for uniform and μ_H-adaptive anisotropic mesh-refinement, where we chose $\theta = 0.5$ in Algorithm 3.3 for the marking strategy and $\tau = 0.5$ to steer the anisotropic mesh-refinement. A comparison with Figure 10 shows that anisotropic (instead of isotropic) mesh-refinement is necessary (and sufficient) to retain the optimal order of convergence.

Figure 13 shows the meshes $\mathcal{T}_h^{(17)}$ with $N = 11.349$ elements generated by μ_H-adaptive isotropic mesh-refinement and $\mathcal{T}_h^{(17)}$ with $N = 2.403$ elements obtained by μ_H-adaptive anisotropic mesh-refinement. We observe strong refinements towards all edges.

Considering the constants $C_{\rm rel}$, C_η, and C_μ as defined in (5.3) we observe that C_η and C_μ behave very similar to the constants obtained in Screen Problem 5.4.

5.6. Empirical Observations on Computational Times. We have observed that the proposed Algorithm 3.3 steered by μ_H, enhanced in 3D by the anisotropic strategy, leads to the optimal order of convergence for the lowest-order Galerkin scheme. However, in practice, computational time is a significant issue in boundary element methods. To compare the computational time t_ℓ for uniform and adaptive mesh-refinment, we proceed as follows:

- For uniform mesh-refinement, we define $t_\ell^{\rm unif}$ as the overall time for ℓ successive uniform mesh-refinements plus the time for the assembly and solution of the Galerkin system.
- For adaptive computations, the ℓ-th solution depends of the entire history of solutions. To reflect this fact, we define the computational time in this case in an inductive way: With $t_{-1}^{\rm adap} := 0$, $t_\ell^{\rm adap}$ is the sum of $t_{\ell-1}^{\rm adap}$ plus the computational time for the assembly

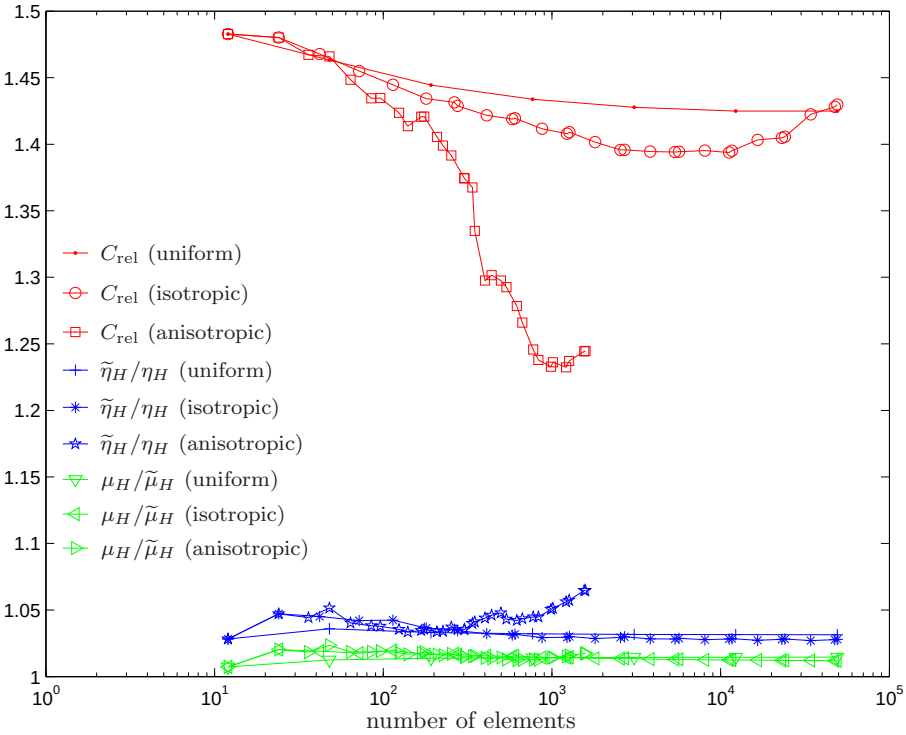

FIGURE 12. Experimental reliability constant $C_{\rm rel} = |||\phi - \phi_h|||/\eta_H$ as well as quotients $C_\eta = \widetilde{\eta}_H/\eta_H$ and $C_\mu = \mu_H/\widetilde{\mu}_H$ in Screen Problem 5.4 for uniform as well as μ_H-adaptive isotropic and anisotropic mesh-refinement.

and the solution of the Galerkin system, the computation of the error estimators, and the refinement of the marked elements.

In Figure 16, we plot the error $|||\phi - \phi_h^{(\ell)}|||$ over the corresponding computational time t_ℓ for both 3D experiments. On a first glance, this comparison may seem to favor the uniform mesh-refinement, since for the ℓ-th adaptive step, we measure the time to compute $\phi_h^{(\ell)}$ and $\phi_{h/2}^{(\ell)}$, but we only plot $|||\phi - \phi_h^{(\ell)}|||$ although the better approximation $\phi_{h/2}^{(\ell)}$ is available. Nevertheless, we see that even for a low accuracy $|||\phi - \phi_h||| \approx 10^{-1}$, the adaptive schemes are superior to uniform mesh-refinement. Besides the optimal convergence order, we observe that adaptive anisotropic mesh-refinement even leads to the best behaviour with respect to the computational cost necessary to reach a certain accuracy.

6. Conclusions and Remarks

6.1. Analytical Results. In this paper, we derived a posteriori error estimators for the Galerkin boundary element method by use of the well-known h-$h/2$-strategy. For the weakly singular integral equation, we provided estimators μ_H that are equivalent to the basic error estimator $\eta_H := |||\phi_{h/2} - \phi_h|||$. Here, ϕ_h and $\phi_{h/2}$ are Galerkin solutions with respect to a mesh $\mathcal{T}_h$ and its uniform refinement $\mathcal{T}_{h/2}$. The advantage of the equivalent error estimator μ_H is that the nonlocal energy norm $|||\cdot|||$ is replaced by a mesh-size weighted L^2-norm.

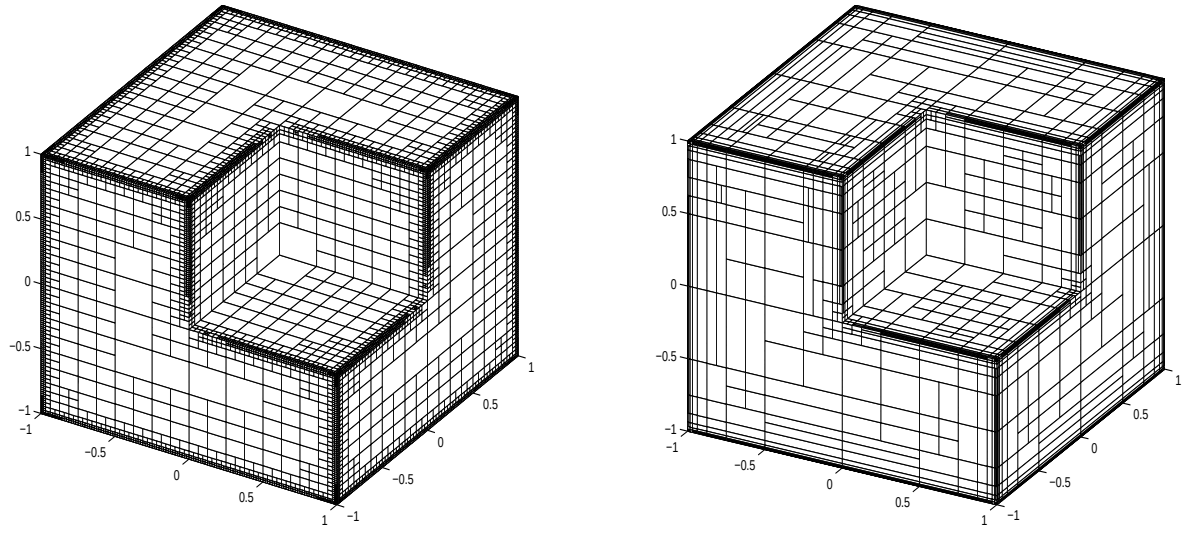

FIGURE 13. Adaptively generated isotropic mesh $\mathcal{T}_h^{(17)}$ with $N = 11.349$ elements (left) in Capacity Problem 5.5 as well as adaptively generated anisotropic mesh $\mathcal{T}_h^{(17)}$ with $N = 2.403$ elements (right). The initial mesh $\mathcal{T}_h^{(0)}$ consisted of $N = 96$ squares with uniform mesh-size $h = \varrho = 1/2$. We observe mesh-refinement along all edges of Γ.

Therefore, the local contributions of μ_H are capable to steer an h-adaptive mesh-refinement. There always holds efficiency

$$\mu_H \lesssim \eta_H \leq |||\phi - \phi_h||| \tag{6.1}$$

under very weak assumptions on the triangulation $\mathcal{T}_h$ used. The converse inequality

$$\eta_H \lesssim \mu_H \tag{6.2}$$

could only be proven for 2D and isotropic mesh-refinement in 3D. More precisely, the constant in this estimate depends on the shape regularity of $\mathcal{T}_h$. Numerical experiments for Symm's integral equation in 3D indicate that this result is too pessimistic in the sense that (6.2) is observed to hold even for anisotropic mesh-refinement. The reliability estimate

$$|||\phi - \phi_h||| \lesssim \eta_H \tag{6.3}$$

depends crucially on the saturation assumption

$$|||\phi - \phi_{h/2}||| \leq C_{\rm sat}\, |||\phi - \phi_h||| \quad \text{with a uniform constant } C_{\rm sat} < 1. \tag{6.4}$$

Contrary to the finite element method, the saturation assumption has not been proven for the boundary element method, yet. However, in all numerical experiments, we got empirical evidence that the saturation assumption holds. This might be due to additional regularity of the exact solution. For instance, all exact solutions appeared to belong not only to the energy space $\widetilde{H}^{-1/2}(\Gamma)$ but also at least to $H^{-\varepsilon}(\Gamma)$, for all $\varepsilon > 0$.

6.2. Advantages of the Proposed Method. Usually, other a posteriori error estimators involve the evaluation of the residual, e.g. [3, 12, 13], or higher-order elements, e.g. [5, 6, 16], and thus need additional implementation. One great advantage of the proposed error

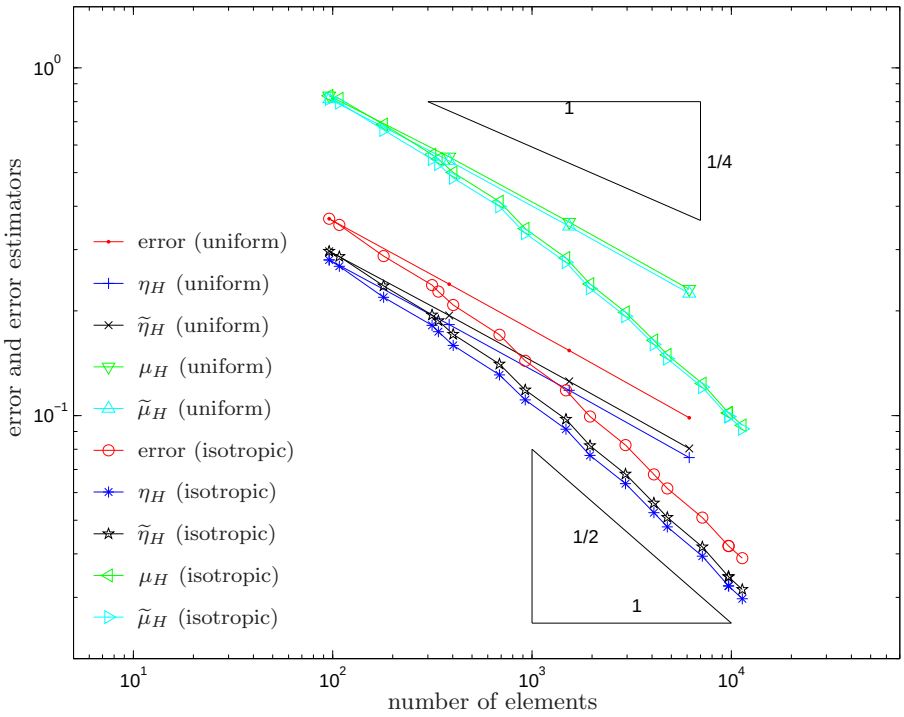

FIGURE 14. Error $|||\phi - \phi_h|||$ and error estimators $\eta_H, \widetilde{\eta}_H, \mu_H, \widetilde{\mu}_H$ in Capacity Problem 5.5 for uniform and μ_H-adaptive isotropic mesh-refinement.

estimators is that there is almost no implementational overhead. Contrary to that, residual-based error estimators usually involve certain quadrature rules to integrate the residual. These quadrature formulae have to deal, by others, with weak singularities according to the integral operator V (and K in case of direct integral formulations).

With respect to the error estimation, we stress that the efficiency estimate for η_H holds with *known* constant $C_{\text{eff}} = 1$ so that η_H gives a concrete lower bound for the unknown error $|||\phi - \phi_h|||$. In the numerical experiments, we observed that the error estimation of η_H is very accurate. The accuracy of η_H is even improved if the mesh $\mathcal{T}_h$ is adaptively generated by the introduced adaptive algorithm. We thus propose to use μ_H to steer the adaptive mesh-refinement and to use η_H for the simultaneous error control.

6.3. Obvious Extensions of the Analysis. Instead of the h-$h/2$-strategy, one can even think of a posteriori error estimators arising from a p-$(p+1)$-strategy: In case of Symm's integral equation with lowest-order boundary elements, let $\phi_{h,0} \in \mathcal{P}^0(\mathcal{T}_h)$ and $\phi_{h,1} \in \mathcal{P}^1(\mathcal{T}_h)$ be Galerkin solutions corresponding to a given triangulation $\mathcal{T}_h = \{T_1, \dots, T_N\}$. As for the h-$h/2$-strategy, we have nestedness of the discrete spaces $\mathcal{P}^0(\mathcal{T}_h) \subset \mathcal{P}^1(\mathcal{T}_h)$ which yields

$$|||\phi - \phi_{h,0}|||^2 = |||\phi - \phi_{h,1}|||^2 + |||\phi_{h,1} - \phi_{h,0}|||^2. \tag{6.5}$$

From this, we infer efficiency of the error estimator

$$\eta_P := |||\phi_{h,1} - \phi_{h,0}||| \le |||\phi - \phi_{h,0}|||. \tag{6.6}$$

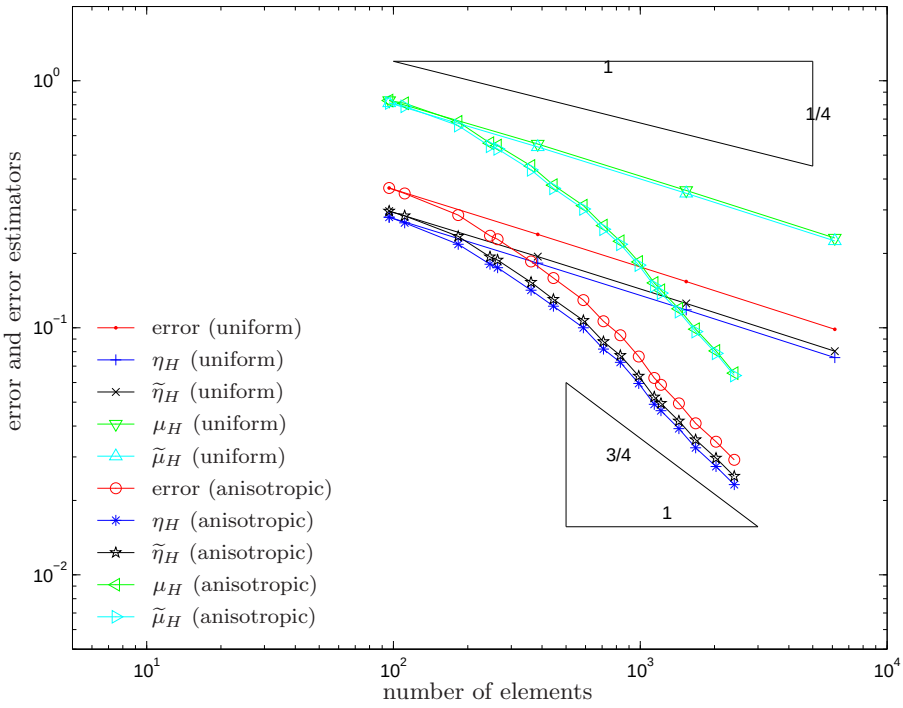

FIGURE 15. Error $|||\phi - \phi_h|||$ and error estimators $\eta_H, \widetilde{\eta}_H, \mu_H, \widetilde{\mu}_H$ in Capacity Problem 5.5 for uniform and μ_H-adaptive anisotropic mesh-refinement, where we chose $\theta = 0.5$ in Algorithm 3.3 for the marking strategy and $\tau = 0.5$ to steer the anisotropic mesh-refinement. A comparison with Figure 14 shows that anisotropic (instead of isotropic) mesh-refinement is necessary (and sufficient) to retain the optimal order of convergence.

As above, the saturation assumption

$$|||\phi - \phi_{h,1}||| \le C_{\rm sat}\, |||\phi - \phi_{h,0}||| \quad \text{with a uniform constant } C_{\rm sat} < 1, \tag{6.7}$$

is equivalent to reliability

$$|||\phi - \phi_{h,0}||| \le \frac{1}{\sqrt{1 - C_{\rm sat}^2}}\, \eta_P. \tag{6.8}$$

Moreover, the same techniques as for η_H apply to prove that the ϱ-weighted error estimator

$$\mu_P := \|\varrho^{1/2}(\phi_{h,1} - \phi_{h,0})\|_{L^2(\Gamma)} \tag{6.9}$$

satisfies $\mu_P \lesssim \eta_P \lesssim \mu_P$, where only the upper estimate depends on the shape regularity of $\mathcal{T}_h$. Numerical experiments and a comparison of the corresponding adaptive strategies are postponed to a forthcoming paper [11].

6.4. Application to Other Integral Equations. Clearly, the idea of this paper works for other elliptic integral operators with energy space $\widetilde{H}^{-1/2}(\Gamma)$ as for, e.g., the Lamé or the Stokes problem. For hypersingular integral operators with energy space $\widetilde{H}^{1/2}(\Gamma)$ and continuous P1-functions, the localization of the energy norm $|||\cdot||| \sim \|\cdot\|_{\widetilde{H}^{1/2}(\Gamma)}$ can be done by nodal interpolation, where we replace Π_h in Lemma 3.1 by the usual nodal interpolation

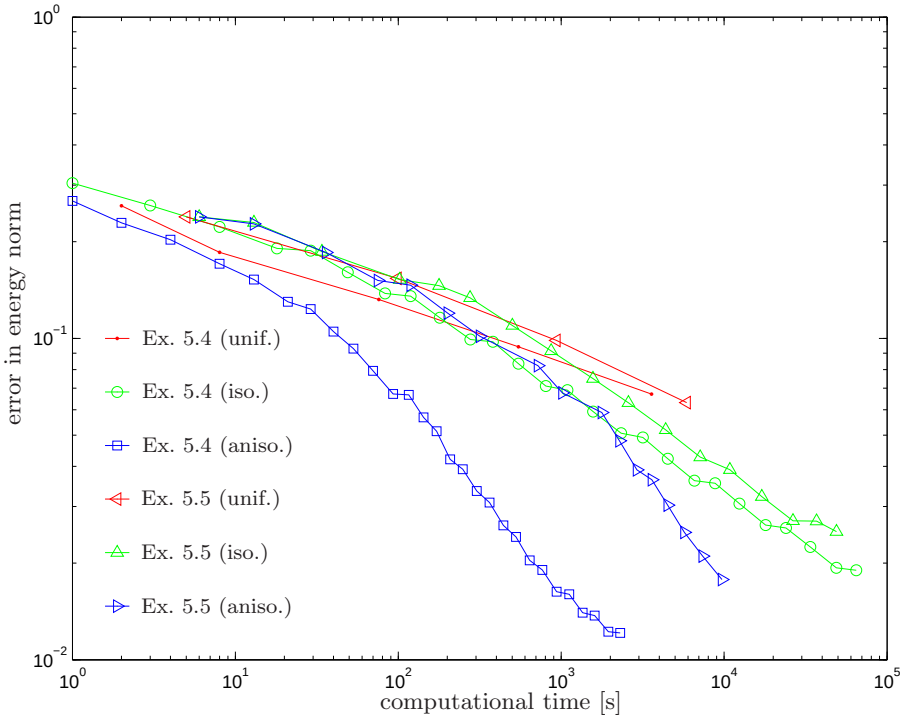

FIGURE 16. Error in the energy norm with respect to the computational time for Examples 5.4–5.5: Besides the optimal convergence order, we observe that adaptive anisotropic mesh-refinement even leads to the best behaviour with respect to the computational cost necessary to reach a certain accuracy.

operator I_h onto $\mathcal{P}^1(\mathcal{T}_h)\cap C(\Gamma)$, cf. [6] for details in 2D. In particular, the h-$h/2$-strategy can even be applied to mixed formulations or transmission problems involving the full Calderón projector, cf. [7, Section 8] in the context of averaging based error estimators.

Acknowledgment. The first author (SFL) acknowledges a grant of the graduate school *Differential Equations – Models in Science and Engineering*, funded by the Austrian Science Fund (FWF) under grant W800-N05. The results of this paper have been presented on the conference *BETA 2007 – Boundary Elements: Theory and Applications*, which took place in May 2007 in Hannover on the occasion of Professor Ernst Stephan's 60th birthday.

REFERENCES

[1] M. BEBENDORF, R. GRZHIBOVSKIS: *Accelerating Galerkin BEM for Linear Elasticity using Adaptive Cross Approximation*, Math. Meth. Appl. Sci. 29 (2006), 1721–1747.

[2] S. BÖRM, L. GRASEDYCK, W. HACKBUSCH: *Introduction to hierarchical matrices with applications*, Eng. Anal. Bound. Elem. 27 (2003), 405–422.

[3] C. CARSTENSEN, M. MAISCHAK, E. STEPHAN: *A posteriori estimate and h-adaptive algorithm on surfaces for Symm's integral equation*, Numer. Math. 90 (2001), 197–213.

[4] C. CARSTENSEN, D. PRAETORIUS: *A Posteriori error control in adaptive qualocation boundary element analysis for a logarithmic-kernel integral equation of the first kind*, SIAM J. Sci. Comp. 25 (2004), 259–283.

[5] C. CARSTENSEN, D. PRAETORIUS: *Averaging techniques for the effective numerical solution of Symm's integral equation of the first kind*, SIAM J. Sci. Comp. 27 (2006), 1226–1260.

[6] C. Carstensen, D. Praetorius: *Averaging techniques for the a posteriori BEM error control for a hypersingular integral equation in two dimensions*, SIAM J. Sci. Comp. 29 (2007), 782–810.
[7] C. Carstensen, D. Praetorius: *Averaging techniques for a posteriori error control in finite element and boundary element analysis*, Springer Lect. Notes Appl. Comput. Mech. 29 (2007), 29–59.
[8] M. Costabel, E. Stephan: *A direct boundary integral equation method for transmission problems.* J. Math. Anal. Appl., 106 (1985), 2, 367–413.
[9] W. Doerfler: *A convergent adaptive algorithm for Poisson's equation*, SIAM J. Numer. Anal. 33 (1996), 1106–1124.
[10] W. Doerfler, R. Nochetto: *Small data oscillation implies the saturation assumption*, Numer. Math. 91 (2002), 1–12.
[11] C. Erath, S. Ferraz-Leite, S. Funken, D. Praetorius: *Energy norm based a posteriori error estimation for boundary element methods in two dimensions*, ASC Report 07/2007, Institute for Analysis and Scientific Computing, Vienna University of Technology, Wien, 2007.
[12] B. Faermann. *Localization of the Aronszajn-Slobodeckij norm and application to adaptive boundary element methods. Part I. The two-dimensional case.* IMA J. Numer. Anal. 20 (2000), 203–234.
[13] B. Faermann. *Localization of the Aronszajn-Slobodeckij norm and application to adaptive boundary element methods. Part II. The three-dimensional case.* Numer. Math. 92 (2002), 467–499.
[14] S. Ferraz-Leite, C. Ortner, D. Praetorius: *Adaptive boundary element methods, simple error estimators and convergence*, Oberwolfach Workshop on Analysis of Boundary Element Methods, Oberwolfach Report 19/2008 (2008), 39–42.
[15] I.G. Graham, W. Hackbusch, S.A. Sauter: *Finite elements on degenerate meshes: Inverse-type inequalities and applications*, IMA J. Numer. Anal. 25 (2005), 379–407.
[16] S. Ferraz-Leite, S. Funken, D. Praetorius: *Averaging on large patches for integral equations in 3D*, work in progress 2008.
[17] M. Maischak: *The analytical computation of the Galerkin elements for the Laplace, Lamé and Helmholtz equation in 2D BEM*, Preprint (1999), *3D BEM*, Preprint (2000), Institute for Applied Mathematics, University of Hannover.
[18] W. McLean: *Strongly elliptic systems and boundary integral equations*, Cambridge University Press, Cambridge 2000.
[19] S. Sauter, C. Schwab: *Randelemente, Analyse und Implementierung schneller Algorithmen*, Teubner Verlag, Stuttgart 2004.

Institute for Analysis and Scientific Computing, Vienna University of Technology, Wiedner Hauptstrasse 8-10, A-1040 Vienna, Austria

E-mail address: {Samuel.Ferraz-Leite,Dirk.Praetorius}@tuwien.ac.at

Correspondence to: Dirk.Praetorius@tuwien.ac.at